Coupled-cluster approach to electron correlation in one dimension: Cyclic polyene model in delocalized basis

J. Paldus,* M. Takahashi,† and R. W. H. Cho‡
Department of Applied Mathematics, University of Waterloo, Waterloo, Ontario, Canada N2L 3G1
(Received 29 June 1984)

The many-electron correlation problem for metalliclike systems with Born—von Kármán boundary conditions, as modeled by the cyclic polyene Pariser-Parr-Pople and Hubbard Hamiltonians, is examined over the entire range of the coupling constant using the coupled-pair (CP) many-electron theory based on the exponential-cluster ansatz for the exact wave function. It is shown that the standard CP theory breaks down not only in the highly correlated, but even in the intermediately correlated, regions, and the nature of its singular behavior in these regions is examined. This breakdown is linked with the increasingly important role played by the connected quadruply excited clusters, which invalidate the basic assumption of the CP theory, as the highly correlated limit and/or the extended character of the model are approached. The contribution from the quadruply excited clusters is then taken into account using the new version of the approximate coupled-pair theory corrected for connected quadruply excited clusters, called ACPQ. This approximation is almost identical with the standard approximate coupled-pair (ACP) -theory approach, in which only factorizable (with respect to hole pairs) nonlinear terms are retained, and differs from it only by a numerical factor associated with one of the nonlinear diagrams. It is shown that the ACPQ not only removes the singularities and associated convergency problems of the standard CP approaches, but, in fact, provides excellent quantitative results over the entire range of the coupling constant, yielding the exact correlation energy in the strongly correlated limit.

I. INTRODUCTION

The problem of electron correlation in extended one-dimensional systems has received the continuous attention of solid-state physicists, theoretical chemists, and mathematical physicists alike ever since the early days of quantum mechanics. Initially, the main reason for the study of such systems was their greater simplicity as compared to their three-dimensional analogs. This, in turn, often enabled the exact solution to be found by exploiting some very elegant mathematics, so that these systems became of interest *per se* for mathematical physicists.[1] The one-dimensional models can often shed useful light on the corresponding three-dimensional problems, even though, more often than not, the basic physical phenomena in one-dimension are radically different from their three-dimensional counterparts.[1] Interested readers can find a vast amount of literature on various one-dimensional model systems as well as some excellent monographs[1,2] and proceedings of specialized meetings.[3]

A renewed interest in these systems was stimulated by the synthesis of polyacetylene films,[4] the highly anisotropic electric conductivity of which can be changed by almost 20 orders of magnitude by doping with small amounts of oxidizing agents,[5] and which possess a number of very fascinating optical, electric, and magnetic properties.[5,6] Even though the initial model explaining some of these properties was based on a strictly one-electron model,[7] the importance of electron correlation in these systems was recognized long ago in connection with the optical properties of linear polyenes.[8–10] Recently, this problem was examined by many authors, exploiting very diverse methods for the handling of electron correlation, particularly in connection with the so-called Peierls instability or chain-dimerization problems.[11–20] A majority of these studies exploited semiempirical model Hamiltonians, either of the Hubbard or Pariser-Parr-Pople (PPP) types (cf., e.g., Ref. 17), and examined both finite and infinite variants of the cyclic or linear polyene models. In fact, as a number of studies indicate, there is little difference between the finite and infinite models, the former ones reaching the "saturation" limit rather quickly with their increasing size.[18,20–22] Recently, these systems were also examined at the *ab initio* level, be it simple chains of H atoms[22–24] or more realistic linear polymer models.[25,26] Several of these investigations went beyond the independent-particle [Hartree-Fock (HF)] approximation, primarily exploiting finite-order perturbation theory,[26] and very recently the multiparametric alternant-molecular-orbital (AMO) method.[27] For the semiempirical Hamiltonians a number of other techniques have been also employed. In particular, several authors[11,14,16,20] start from the homopolar valence-bond (VB) picture, which is most appropriate for the fully correlated limit, even though the ionic VB states become more and more important as the intermediately correlated region is approached. However, in contrast to the three-dimensional electron-gas problem, where a number of various infinite-order perturbation-theory approaches, ranging from the random-phase approximation (RPA) to the approximate coupled-cluster (CC) approach, have been successfully applied,[28,29] no papers exist exploiting the infinite-order techniques in one-dimension. The reason for this fact probably lies in the truly singular character of the one-

dimensional correlation problem, in which the electrons are subject to "head-on" collisions and which causes various divergence or singularity problems when standard applications are made, as we shall see below. Only a very recent development in the coupled-cluster approach[30] enabled us to better understand this model and to overcome these divergence and singularity problems.

In this paper we first apply the standard coupled-pair many-electron theory (CPMET),[31] briefly outlined in Sec. II, to the linear metallic chain, modeled by the cyclic polyene semiempirical Hamiltonians of both PPP and Hubbard type, which are described in Sec. III. It is shown that the CPMET suffers from a singular behavior (Sec. IV) when the length of the chain becomes large, or for chains with 14 or more sites, when the strongly correlated limit is approached. The full range of the coupling constant is always considered. We next examine the nature of this singularity in Sec. V, while Sec. VI contains the results which, in addition to the pair clusters, also account for quadruply excited connected clusters using the technique described in greater detail in Ref. 30. This new method, which is computationally almost identical with the approximate coupled-pair (ACP) approach,[32–34] yields excellent results over the entire range of the coupling constant and becomes exact in the fully correlated limit for both the PPP and the Hubbard Hamiltonians. In Sec. VII these results are discussed from the viewpoint of the general correlation problem in one-dimensional systems. The essential role played in these systems by the connected quadruply excited clusters is clearly shown, and the new ACPQ (denoting the new version of the approximate coupled-pair theory corrected for connected quadruply excited clusters) technique which accounts for their effect is tested on this very challenging model.

II. COUPLED-CLUSTER FORMALISM

We now briefly review the notation and formalism of the CC theory as needed in this paper. The essence of the CC approach is to exploit the logarithm of the wave operator, called the cluster operator, thus transforming the multiplicative wave-function structure into the additive one. Since the wave operator is then represented by the exponential map of the cluster operator, we are guaranteed the correct particle number N dependence even when the cluster operator is arbitrarily truncated to the one-or two-body, or, generally, low-order terms. Such a truncation will, of course, be physically meaningful only when the higher-order components can be successfully represented as products of lower-order clusters, which arise via the exponential map. Assuming such a truncation to be viable, one derives the set of (generally) nonlinear CC equations determining the low-order cluster components. These equations essentially represent the recursion formulas for the generation of relevant diagrams of many-body perturbation theory (MBPT), whose contribution is then automatically summed to infinite order by solving the CC equations. The exponential structure of the wave operator was discovered by Hubbard[35] and Hugenholtz,[36] and its exploitation in the nuclear correlation problem was suggested by Coster and Kümmel.[37]

The general equations for CC components, in a form particularly suitable for the atomic and molecular many-electron correlation problem, were given by Čížek.[31,38] During the past decade a number of important developments contributed to a better understanding, and the extension, of the CC approach, as well as to its efficient computational implementation, and their exposition may be found in numerous reviews[39–44] or even monographs.[45] We thus restrict our attention to those closed-shell approaches which are employed in this paper.

Starting with some independent-particle-model (IPM) single determinantal state $|\Phi\rangle$, we write the exact state $|\Psi\rangle$ in the cluster-expanded form (using the intermediate normalization $\langle\Psi|\Phi\rangle=1$)

$$|\Psi\rangle=\exp(\hat{T})|\Phi\rangle\ ,\quad \hat{T}=\sum_{i=1}^{N}\hat{T}_i\ . \tag{1}$$

Using the second-quantization formalism, the i-times-excited (ith-order or i-body) cluster component $\hat{T}_i$ can be expressed through its matrix elements as follows:

$$\hat{T}_i=(i!)^{-1}\sum_{\{A\}}\langle A^1,\ldots,A^i|\hat{t}_i|A_1,\ldots,A_i\rangle \times\prod_{j=1}^{i}(\hat{X}^{\dagger}_{A^j}\hat{X}_{A_j})\ , \tag{2}$$

where $\hat{X}^{\dagger}_A$ ($\hat{X}_A$) designates the creation (annihilation) operators associated with an orthonormal spin-orbital set $\{|A\rangle\}$. This set consists of a disjoint union of the hole $\{|A_i\rangle\}$ and particle $\{|A^i\rangle\}$ spin-orbital subsets, the former determining the IPM reference state $|\Phi\rangle$, $|\Phi\rangle=\prod_i\hat{X}^{\dagger}_{A_i}|0\rangle$, with $|0\rangle$ designating the true physical vacuum state.

The CC equations determining the cluster components $\hat{T}_i$ (that is, the matrix elements

$$\langle A^1,\ldots,A^i|\hat{t}_i|A_1,\ldots,A_i\rangle)$$

are then obtained by employing the cluster ansatz, Eq. (2), in the time-independent Schrödinger equation,

$$\hat{H}_N|\Psi\rangle=\Delta\epsilon|\Psi\rangle\ , \tag{3}$$

which we have written in the normal product form[31,46] with $\Delta\epsilon$ designating the correlation energy (relative to the IPM energy). We assume that the Hamiltonian of the closed-shell system considered is spin independent and contains, at most, two-body interactions, i.e.,

$$\hat{H}_N=\sum_{a,b}\langle a|\hat{f}|b\rangle N[\hat{E}_{ab}] +\tfrac{1}{2}\sum_{a,b,c,d}\langle a,b|\hat{v}|c,d\rangle N[\hat{E}_{ac}\hat{E}_{bd}]\ , \tag{4}$$

where the N product is defined with respect to $|\Phi\rangle$,[46] and the orbital unitary group generators $\hat{E}_{ab}$ are given by[47]

$$\hat{E}_{ab}=\sum_{\sigma}\hat{X}^{\dagger}_{a\sigma}\hat{X}_{b\sigma}\ , \tag{5}$$

assuming that the spin orbital $|A\rangle$ can be written as a simple product of the orbital and spin states, $|A\rangle$

$=|a\rangle|\sigma\rangle$, $\sigma=\pm\frac{1}{2}$. The one-electron matrix elements are defined by

$$\langle a|\hat{f}|b\rangle=\langle a|\hat{z}|b\rangle+\sum_{c_1}(2\langle a,c_1|\hat{v}|b,c_1\rangle - \langle a,c_1|\hat{v}|c_1,b\rangle), \quad (6)$$

the sum extending over the hole-state orbitals (distinguished by subscripts from the particle labels, which carry a superscript).

Substituting the cluster expansion, Eq. (1), into Eq. (3), and exploiting the time-independent diagrammatic formalism,[46] we obtain

$$[\hat{H}_N\exp(\hat{T})|\Phi\rangle]_C=\Delta\epsilon|\Phi\rangle, \quad (7)$$

where the subscript C indicates that only connected diagrams are to be considered. Projecting this equation onto the IPM state $|\Phi\rangle$, we obtain the correlation energy expression

$$\Delta\epsilon=\langle\Phi|\hat{H}_N\exp(\hat{T})|\Phi\rangle_C=\langle\Phi|\hat{H}_N(\tfrac{1}{2}\hat{T}_1^2+\hat{T}_2)|\Phi\rangle_C, \quad (8)$$

and the energy-independent CC equations follow from a similar projection onto the appropriate manifold of κ-times-excited configurations $|\Phi_i^{(\kappa)}\rangle$,

$$\langle\Phi_i^{(\kappa)}|\hat{H}_N\exp(\hat{T})|\Phi\rangle_C=0, \quad \kappa=1,2,\ldots,k. \quad (9)$$

Since the pair clusters $\hat{T}_2$, which already appear in first-order MBPT, play the most important role, the commonly used truncation scheme is to assume that $\hat{T}\approx\hat{T}_2$ (or $\hat{T}\approx\hat{T}_1+\hat{T}_2$ if the $\hat{T}_1$ are not negligible). The coupled-pair many-electron theory (CPMET), or simply CCD (coupled clusters with doubles), equations[31,38,48] determining the $\hat{T}_2$ component are then obtained by considering the doubly excited manifold $\{|\Phi_i^{(2)}\rangle\}$ in Eq. (9).

We shall find it particularly convenient to employ the so-called orthogonally-spin-adapted form of the CCD equations in which the pair-cluster matrix elements as well as the projection in Eq. (9) are defined with respect to an orthogonal set of singlet pp-hh coupled biexcited configurations,[49]

$$\left|\begin{matrix}a^1 & a^2\\ a_1 & a_2\end{matrix}\right\rangle_S,$$

where the subscripts S ($S=0,1$) designates the intermediate spin of pp (hh) pairs. These configurations, as well as the corresponding $\hat{t}_2$ matrix elements, $\langle a^1,a^2|\hat{t}_2|a_1,a_2\rangle_S$, possess very simple and desirable properties given by Eqs. (22), (23), and (29)—(31) of Ref. 50. The explicit form of the CC equations[50] in orthogonally-spin-adapted form is most simply derived by applying the diagrammatic time-independent technique[46] combined with graphical methods of spin algebras (cf., e.g., Refs. 45, 49, and 51). For convenience and for purposes of further discussion, the relevant orbital diagrams and orthogonally adapted CCD equations are given in Appendix A. Assuming some fixed but arbitrary ordering of the $\hat{t}_2$ matrix elements, we can simply label them [or the corresponding unnormalized $\hat{\tau}_2$ matrix elements, Eq. (A1)] by t_i ($i=1,\ldots,m$), where m is the number of linearly independent pair clusters considered. The CCD equations can then be cast into the following simple form:

$$a_i+b_{ij}t_j+c_{ijk}t_jt_k=0, \quad (10)$$

assuming the summation is over repeated indices. The coefficients a_i, b_{ij}, and $c_{ijk}=c_{ikj}$ are given by the expressions of Appendix A in terms of one- and two-electron integrals $\langle a|\hat{f}|b\rangle=\delta_{ab}\epsilon_a$ and $\langle a,b|\hat{v}|c,d\rangle$, respectively, defined in terms of the orthonormal HF (or, generally, IPM) molecular-orbital basis.

Neglecting the nonlinear part (i.e., setting $c_{ijk}=0$) in Eq. (10), we obtain the linear version of the coupled-pair theory designated as the L-CCD approach. The relationship of this approximation with the configuration-interaction approach limited to biexcited configurations (DCI) was studied in detail in Ref. 52.

We shall also consider an approximation[32—34] in which only the nonlinear diagrams 4 and 5 [cf. Fig. 10(c) in Appendix A], namely those which factorize with respect to hole pairs, are considered. This approximation, referred to as the ACP-D45 (approximate coupled pairs with diagrams 4 and 5), or simply the ACP, approach, was shown to yield results very close to the full CCD approach in both semiempirical[32] and *ab initio*[32—34,53] applications. In fact, this approximation provides results which are usually better than the full CCD approach, particularly in quasi-degenerate situations.[32,54] This fact was recently explained[30] by considering the corrections to the CCD equations accounting for the effect of connected tetraexcited clusters, which effectively eliminate the contribution from the first three nonlinear diagrams (D123) [Fig. 10(c) in Appendix A]. These corrections are given by the term

$$\Lambda^{(3)}=\langle\Phi_i^{(2)}|\hat{H}_N\hat{T}_4|\Phi\rangle_C,$$

which is neglected in the CCD approach, and we have estimated its contribution by approximating the $\hat{T}_4|\Phi\rangle$ component by the connected quadruply excited component which is contained in the unrestricted Hartree-Fock (UHF) wave function or some of its projected versions, such as the projected Hartree-Fock[55] (PHF) or the alternant-molecular-orbital[56,57] method. One can, in fact, exploit the general structure of the UHF solution to derive the general form of an approximation for $\Lambda^{(3)}$ (Ref. 30). This approximation would be exact if the UHF wave function were exact. The resulting approximate coupled-pair procedure, which thus approximately accounts for connected quadruple clusters, is designated as the ACPQ approach,[30] and is found to be almost identical to the ACP-D45 approach[32—34] mentioned above, except for the numerical factor of 9 associated with the diagram 5 [Fig. 10(c)] contribution to those CCD equations, which are obtained by the projection onto doubly excited configurations with intermediate triplet coupling of hh and pp pairs. [Note that in these CCD equations diagram 5 gives a nonvanishing contribution only to products of triplet coupled cluster components, as follows immediately from the last term in Eq. (A5), in which $\tilde{S}$ appears in every $\hat{\tau}_2$

term.] We shall see that this modification of the CPMET or the CCD approach, which accounts for the $\hat{T}_4$ component, will prove to be of the utmost importance for the applications of the CC approach to cyclic polyenes and to highly degenerate situations in general.

III. CYCLIC POLYENE MODEL

We consider the cyclic polyenes C_NH_N with the nondegenerate ground state[58] ($N=2n=4\nu+2$, $\nu=1,2,\ldots$) described by the model Pariser-Parr-Pople Hamiltonian[59] $\hat{H}_\pi$,

$$\hat{H}_\pi=\sum_{\mu,\nu} z_{\mu\nu}\hat{E}_{\mu\nu}+\tfrac{1}{2}\sum_{\mu,\nu}\gamma_{\mu\nu}(\hat{E}_{\mu\mu}\hat{E}_{\nu\nu}-\delta_{\mu\nu}\hat{E}_{\mu\nu}) , \quad (11)$$

where the orbital unitary group, $U(N)$, generators $\hat{E}_{\mu\nu}$ are defined by Eq. (5) and the creation and annihilation operators of the second-quantization formalism are defined on a minimum basis set of atomic spin orbitals $|\mu,\sigma\rangle=|\mu\rangle\,|\sigma\rangle$, $\mu=0,1,\ldots,N-1$, $\sigma=\pm\frac{1}{2}$, localized on the vertices of the regular N-gon. This Hamiltonian results from the general π-electron Hamiltonian by invoking the approximation of zero differential overlap,[59] so that only two-center Coulomb-type two-electron integrals survive. Like all semiempirical Hamiltonians, it is defined directly by specifying the one- and two-electron matrix elements $z_{\mu\nu}$ and $\gamma_{\mu\nu}$, respectively, rather than by selecting the spin-orbital basis $\{|\mu,\sigma\rangle\}$ as is done for *ab initio* model Hamiltonians.

For the one-electron matrix elements the tight-binding approximation is employed, so that in view of the D_{Nh} symmetry of our model, we have that

$$z_{\mu\mu}=z_0=0 , \quad z_{\mu,\mu\pm1}=\beta , \quad (12)$$

and

$$z_{\mu\nu}=0 \ \text{ otherwise} ,$$

with all indices understood to be taken mod N and where zero of the energy scale is chosen by setting $z_0=0$. The one-electron component of $\hat{H}_\pi$ is thus proportional to the resonance integral β, whose reciprocal value can be interpreted as the coupling constant for this model. Consequently, varying the resonance integral β from zero (fully correlated limit) to large negative values (-5 or -10 eV in practice, weakly correlated limit), we can examine the entire range of the correlation effects. Obviously, the strongly (fully) correlated limit ($\beta=0$) corresponds to the low-density (or strong-coupling, $r_s\to\infty$) regime, using the parlance of the electron-gas model, and, conversely, the weakly correlated limit ($-\beta\to\infty$) corresponds to the high-density ($r_s\to0$) limit. The physical (spectroscopic) value of the resonance integral β for the Coulomb integral approximations used below is about -2.5 eV.

We use the Mataga-Nishimoto[60] parametrization for the two-electron Coulomb repulsion integrals $\gamma_{\mu\nu}$ in the PPP model, with the one-center integral γ_{00} defined through the difference between the valence-state ionization potential and electron affinity (so-called $I-A$ approximation[59]), so that

$$\gamma_{00}=10.84 \text{ eV} ,$$
$$\gamma_{\mu\nu}=e^2/(R_{\mu\nu}+a) , \quad a=e^2/\gamma_{00} \quad (13)$$

where $R_{\mu\nu}$ is the internuclear separation between the sites μ and ν. The nearest-neighbor site separation is taken to be 1.4 Å. For the Hubbard model, in which only on-site interactions are allowed, we have simply

$$\gamma_{\mu\nu}=\gamma\delta_{\mu\nu} , \quad (14)$$

with $\gamma=5$ eV (roughly equaling the $\gamma_{00}-\gamma_{01}$ difference for the PPP model Hamiltonian; cf. Ref. 61). The geometry of our model again implies that

$$\gamma_{\mu\nu}=\gamma_{\mu+\kappa,\nu+\kappa}=\gamma_{0,\mu-\nu} . \quad (15)$$

Including the internuclear repulsion term[59] $\sum_{\mu<\nu}\gamma_{\mu\nu}$, we can write the Hamiltonian (11) in the following simple form:

$$\hat{H}=\beta\sum_{\mu}(\hat{E}_{\mu,\mu+1}+\hat{E}^{\dagger}_{\mu,\mu+1})+\tfrac{1}{2}\sum_{\mu,\nu}\gamma_{\mu\nu}(\hat{n}_\mu-1)(\hat{n}_\nu-1) , \quad (16)$$

where $\hat{n}_\mu=\hat{E}_{\mu\mu}$ is the μth-site occupation-number operator.

The Hartree-Fock molecular orbitals $|k\rangle$, $k=0,1,\ldots,N-1$, are given by Bloch's theorem,

$$|k\rangle=N^{-1/2}\sum_{\mu=0}^{N-1}\exp(i\omega k\mu)\,|\mu\rangle , \quad \omega=2\pi/N \quad (17)$$

and the corresponding one- and two-electron integrals take a very simple form when transformed to this basis, namely (cf. e.g., Ref. 21)

$$\langle k\,|\,\hat{z}\,|\,l\rangle=2\beta\,\delta_{kl}\cos(\omega k) , \quad (18)$$

$$\langle k,l\,|\,\hat{v}\,|\,k',l'\rangle=K(k-k')\delta_{k+l,k'+l'} , \quad (19)$$

where

$$K(k)=K(-k)=N^{-1}\sum_{\mu=0}^{N-1}\gamma_{0\mu}\exp(i\omega k\mu) ,$$
$$k=0,1,\ldots,n \quad (20)$$

with all indices or arguments taken mod N. The Hartree-Fock orbital energies ϵ_k are

$$\epsilon_k=\langle k\,|\,\hat{f}\,|\,l\rangle\delta_{kl}=2\beta\cos(\omega k)+NK(0)-\sum_{k_1}K(k-k_1) , \quad (21)$$

where the summation extends over the occupied (hole) orbital set labels k_1,

$$-\nu\le k_1\le\nu , \quad (22)$$

defining the HF sea. Thus, the Bloch orbitals (17) are pairwise degenerate, $\epsilon_k=\epsilon_{-k}\equiv\epsilon_{N-k}$, except when $k=0$ or n. We also note that the exact solutions for the first two members ($N=6$ and 10) are available,[17] as well as those for both the Hubbard finite[62] and infinite[63] models.

In addition to the spatial C_N or D_{Nh} symmetry, these models also possess the hole-particle and so-called alter-

nancy symmetries.[59,61] The natural label for the symmetry species of the C_N subgroup is the quasimomentum k labeling Bloch orbitals, Eq. (17). Since the Bloch orbitals (17) are completely determined by the symmetry for our models, with each Bloch orbital spanning one irreducible representation of C_N, they are simultaneously both the HF and Brueckner (maximum-overlap) orbitals. Consequently, all monoexcited $\hat{T}_1$ clusters, which are invariably associated with a nonzero quasimomentum transfer, must vanish, since our cyclic polyene models have a nondegenerate totally symmetric ground state which is characterized by zero quasimomentum. Thus the CCD approach is, in this case, equivalent to the CC with singles and doubles (CCSD) approach. However, triexcited or higher odd-number-of-times—excited clusters do not necessarily vanish and do give a nonvanishing contribution to the correlation energy.

The pair clusters must also be associated with an overall zero quasimomentum. In view of the cyclic symmetry the n^4 dependence for the number of all biexcited configurations (or pair clusters) reduces to the n^3 dependence since a general $\hat{t}_2$ matrix element with a vanishing quasimomentum has the form

$$\langle a^1,a^2 \mid \hat{t}_2 \mid a^1-k\ ,a^2+k\rangle_S\ , \tag{23}$$

where $a_1=a^1-k$ and $a_2=a^2+k$ must be hole labels (mod N), i.e., $-\nu\le a_i\le\nu$, $i=1,2$. Each such matrix element is uniquely specified by the virtual orbital labels a^1,a^2 and the quasimomentum transfer k (together with the intermediate-spin label S, of course).

In order to exploit the p-h and alternancy symmetries, we represent Bloch orbitals by the vertices of a regular N-gon with its center at the origin of a Cartesian system (cf. Fig. 1), also displaying the orbital degeneracies since the ordinates of each vertex give corresponding one-particle energies, Eq. (18). The h-p pairing then corresponds to a reflection in the horizontal x axis, while the

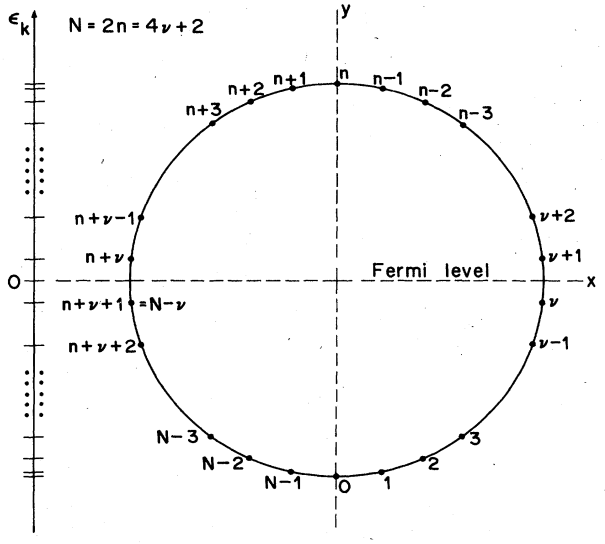

FIG. 1. Schematic representation of the Bloch-orbital labeling, corresponding one-electron energies, and hole-particle (h-p), complex conjugation, and alternancy symmetries as represented by reflections in the x axis, y axis, and the origin, respectively.

y-axis reflection is associated with complex conjugation. The alternancy conjugation results in the multiplicative phase factor $\exp(i\omega n\mu)=(-1)^\mu$ applied to each $|\mu\rangle$ atomic orbital in each Bloch orbital, Eq. (17), which changes the signs of all the odd coefficients. This operation clearly corresponds to the operation of inversion in the origin using the representation of Fig. 1. Equivalently, the alternancy conjugation corresponds to adding the maximal quasimomentum transfer $k=n$ to the orbital label. These additional symmetries can further reduce the number of independent $\hat{t}_2$ matrix elements (they cannot, however, change their cubic dependence, but only to lower the multiplicative coefficient at n^3).

We have exploited all available symmetries by first systematically enumerating the elements (23) for each quasimomentum transfer k while deleting duplications which follow from the p-h conjugation. Thus, for $k=1,2,\ldots,\nu+1$ the virtual pairs a^1,a^2 will range from $a^1=\nu+1$ to $a^1=\nu+k$ (or $a^1=\nu+r+1$ if $q=r$ and k is odd) with a^2 given by $a^2=\nu+n-q$, for each $q=0,1,\ldots,r$, with $r=[\frac{1}{2}(k-1)]$ (here, $[x]$ designates the integer part of x). For each k ($k\le\nu+1$), we thus obtain $\bar{m}_k$ matrix elements,

$$\bar{m}_k=[\tfrac{1}{2}(k^2+1)]\ ,\quad k=1,\ldots,\nu+1\ . \tag{24}$$

For quasimomentum transfers k, $k>\nu+1$, the above list will partially duplicate already listed elements (e.g., $\langle\nu+1,\ 3\nu+1\mid\hat{t}_2\mid-1,\ 1\rangle_S$, with $k=\nu+2$, is equivalent to $\langle\nu+1,\ 3\nu+1\mid\hat{t}_2\mid 1,\ -1\rangle_S$ with $k=\nu$). We can eliminate these duplications by ranging a^1 from $a^1=\max(\nu+1,\nu+2k+n-q)$ to $a^1=\min(\nu+k,n+\nu-q)$ (or, again, $a^1=\nu+r+1$ if $q=r$ and k is odd), with $a^2=n+\nu-q$, $q=0,1,\ldots,r=[\frac{1}{2}(k-1)]$. Thus, for each $k=\nu+2,\ldots,n$ we now have only $\bar{m}_k$ t_2 elements,

$$\begin{aligned}&\bar{m}_k=[\tfrac{1}{2}(k^2+1)]-k'(2k'+1),\\ &k'=k-\nu-1\quad(k>\nu+1)\ .\end{aligned} \tag{24'}$$

The total number of singlet coupled ($S=0$) $\hat{t}_2$ matrix elements, $\bar{m}_{(S=0)}$, which follows from this enumeration is

$$\bar{m}_{(S=0)}=\sum_{k=1}^{n}\bar{m}_k\ , \tag{25}$$

with $\bar{m}_k$ given by Eqs. (24) and (24') (see Table I). The triplet coupled pair clusters are fewer in number since both hole and particle labels must be distinct ($a^1\neq a^2$, $a_1\neq a_2$) (see Table I). Further reduction is then possible, exploiting fully the alternancy and orbital-conjugation symmetries by simply carrying out both symmetry operations on each listed element and searching for duplications. An efficient indexing scheme for the pair clusters can then be developed using the above-listed enumeration.[64] The resulting number (and, in fact, an actual list) of independent pair clusters for both spin couplings, as well as their sum m_T which gives the order of the system of CCD nonlinear equations (10), are listed in Table I for the first seven polyenes. It can be shown that, in the limit of $N=2n\to\infty$, the number of zero-quasimomentum biexcitations will vary as $\frac{2}{3}n^3$. Exploiting all the available

TABLE I. Dimension of the pair-cluster manifolds for cyclic polyenes C_NH_N, $N=4\nu+2$, with various degrees of symmetry adaptation. The number $\overline{m}_{(S=0)}$ gives the dimension of biexcitation manifold with singlet intermediate coupling which follows from the enumeration given by Eq. (25), while $m_{(S=0)}$ and $m_{(S=1)}$ are dimensions for singlet and triplet intermediate couplings, respectively, when all the available symmetries of the PPP cyclic polyene model are exploited. The last row gives the total number m_T of $\hat{t}_2$ matrix elements, $m_T=m_{(S=0)}+m_{(S=1)}$, and thus the order of the system of CCD equations, Eq. (10).

$\nu=$	1	2	3	4	5	6	7
$N=$	6	10	14	18	22	26	30
$\overline{m}_{(S=0)}$	5	16	38	75	131	210	316
$m_{(S=0)}$	5	14	30	55	91	140	204
$m_{(S=1)}$	2	8	20	40	70	112	168
m_T	7	22	50	95	161	252	372

symmetry yields an additional factor of $\frac{1}{4}$, so that the overall number of totally symmetric biexcitations varies as $n^3/6$.

The above-listed symmetry properties will also simplify the CCD equations (A2)—(A8). Roughly, each $\hat{t}_2$ matrix element will eliminate one orbital summation. This particularly facilitates the computations of the nonlinear part since it reduces the fourfold summations in Eq. (A5) to only twofold sums.[64] For example, the most laborious first term in Eq. (A5), which we write schematically as

$$\sum_{b_1',b_2',b_1'',b_2''} \langle b_1',b_2' \,|\, \hat{v} \,|\, b_2'',b_1'' \rangle \sum_{S,S',\kappa} G(S,S_1',\kappa) \langle a_1'',b_1'' \,|\, \hat{\tau}_2 \,|\, a_\kappa',b_1' \rangle_S \langle a_2'',b_2'' \,|\, \hat{\tau}_2 \,|\, a_{\bar{\kappa}}',b_2' \rangle_{S'} , \tag{26}$$

where $G(S,S',\kappa)$ designates the remaining $\tilde{S}$-, S-, S'-, and κ-dependent factors, reduces to

$$\sum_{b_1',b_2'} \langle b_1',b_2' \,|\, \hat{v} \,|\, b_2'',b_1'' \rangle \sum_{S,S',\kappa} G(S,S',\kappa) \langle a_1'',b_1'' \,|\, \hat{\tau}_2 \,|\, a_\kappa',b_1' \rangle_S \langle a_2'',b_2'' \,|\, \hat{\tau}_2 \,|\, a_{\bar{\kappa}}',b_2' \rangle_{S'} , \tag{26'}$$

where

$$b_1''=a_\kappa'+b_1'-a_1''(\mathrm{mod}\,N) , \quad b_2''=a_{\bar{\kappa}}'+b_2'-a_2''(\mathrm{mod}\,N) . \tag{26''}$$

Extreme care, however, must be exercised when applying various approximation procedures while employing the symmetry simplifications indicated above. For example, it is immediately obvious that the nonlinear diagrams 3 and 4 [Fig. 10(c)] are related by hole-particle symmetry (i.e., the reversal of the orientation of each fermion line transforms one into the other). Now, for the cyclic polyene model, which possesses h-p symmetry, both diagrams 3 and 4 [Fig. 10(c)] yield identical contributions. Now, if we apply the ACP approximation, for example, in which only diagrams 4 and 5 [Fig. 10(c)] are considered, this p-h symmetry will be broken. Consequently, an exploitation of h-p (or, closely related to it, alternancy) symmetry in our calculations would lead to an incorrect result. An obvious way to circumvent this problem is, of course, to ignore the alternancy or p-h symmetries and to exploit only the spatial symmetry. We have found, however, that an almost equivalent result (up to at least three decimal figures in the strongly correlated limit and to seven decimal figures in the weakly correlated region) is obtained when keeping other than spatial symmetries (thus reducing the order of the problem by roughly a factor of 4), but replacing each diagram contribution by its average over all the configurations which are generated from those appearing explicitly by the p-h and alternancy conjugations. In this way the maximal symmetry reduction can still be exploited even when the approximate ACP and ACPQ approaches are used.

IV. COUPLED-PAIR RESULTS

We have written a special-purpose program, exploiting all the available symmetries of the PPP cyclic polyene models, along the lines outlined in the preceding section. This significantly reduces the computational complexity, so that even for a fairly large cycle such as $N=22$ polyene, the order of the CCD equations was only 161. Thus, the linear system of the L-CCD equations was solved using the Gauss elimination algorithm, and a standard Newton-Raphson procedure [cf., e.g., Appendix B of Ref. 33(a)] was sued to solve the nonlinear CCD system, Eq. (10). In normal cases, only three or at most five Newton-Raphson iterations were needed to obtain at least the seven-figure accuracy.

As we have shown earlier, the L-CCD approximation breaks down when the lowest-lying canonical biexcitation becomes degenerate with the reference configuration.[52] For the cyclic polyene models this will invariably happen when we approach the strongly correlated limit, and the critical value of the coupling constant for this to happen is given by the resonance-integral (β) value which makes

the matrix $\underline{B}=||b_{ij}||$ singular. Since the resonance integral β occurs only linearly in the diagonal terms, it is easy to find this critical value, $\beta_c^{\text{L-CCD}}$, by diagonalization [cf. the Appendix of Ref. 18(a)]. Of course, we can also simply interpolate to find $\beta_c^{\text{L-CCD}}$ for which the lowest eigenvalue of $\underline{B}$ vanishes. This critical value $\beta_c^{\text{L-CCD}}$ of the resonance integral is shifted towards the weakly correlated limit with increasing polyene size N (cf. Fig. 2). Thus, while the L-CCD approximation can provide reasonable values of the correlation energy for the intermediately strong coupling in small rings (cf. Tables II—V), it will invariably break down, even in the intermediately correlated region, as $N\rightarrow\infty$ (cf. Figs. 3—6). Moreover, higher and higher eigenvalues of $\underline{B}$ will cross zero and become negative as $\beta\rightarrow 0$ or as $N\rightarrow\infty$ (cf. Fig. 2), so that the L-CCD approximation will possess a highly singular character in the crucial intermediate- and strong-coupling regions. For the smallest ring ($N=6$), at most two roots of $\underline{B}$ can vanish as $\beta\rightarrow 0$, namely at $\beta_c^{\text{L-CCD}}=-0.79$ eV and $\beta_c{}'^{\text{L-CCD}}=-0.37$ eV. Dependence of the first few critical resonance integral values on N is illustrated in Fig. 2.

Consequently, the L-CCD approximation, which is equivalent to the infinite-order MBPT with doubly excited intermediate states (cf., e.g., Ref. 52), called D-MBPT(∞),[39] will not be usable even as the first approximation in solving the nonlinear CCD equations. In fact, already at about $\beta=-1$ eV (for $N=6$), the Newton-Raphson procedure does not converge when the L-CCD solution is used as the starting iteration. In such cases, one has to use either the second-order perturbation-theory result (given simply by $t_i\sim a_i/b_{ii}$) or the D-CI (configuration interaction restricted to doubly excited configurations) result [obtained by diagonalizing the $\underline{B}$ matrix bordered with $(0,\underline{a})$ and $(0,\underline{a})^{\text{tr}}$, $\underline{a}=||a_i||$, as the first row and column; cf. Ref. 52] as the starting iteration. Even this remedy may fail in the strongly correlated limit, particularly as N increases and both the D-CI and the second-order MBPT become poorer and poorer approximations. Here, the best procedure was to employ as the first approximation the CCD solution for a sufficiently close resonance-integral value, proceeding from the well-behaved, weakly correlated limit where all of the above-mentioned procedures yield a fast convergence in a few (about 3—5) iterations. Using the CCD solution for the sufficiently close β value, and making the steps sufficiently small as $|\beta|$ is decreased, enabled us to find the solution of the CCD equations for the first two cycles ($N=6$ and 10) in the entire region of the coupling constant. However, while the CCD approximation provides an excellent approximation in the weakly and intermediately correlated regions in this case ($N=6$ and 10), it fails in the strongly correlated region, as Figs. 3 and 4, giving the percentage error in the correlation energy, indicate. The situation is very similar for both the PPP and the Hubbard Hamiltonians.

For the $N=14$ ring a procedure analogous to that described above fails at $\beta\approx -1.75$ eV. At this point the correlation energy $\Delta\epsilon$, as well as the most important pair clusters t_i, begin to deteriorate rapidly ($|d\Delta\epsilon/d\beta|\rightarrow\infty$), and even when very small steps in the resonance-integral lowering are used the Newton-Raphson procedure fails to converge. This critical resonance-integral (β) value, beyond which we were unable to find any solution of the CCD equations using our Newton-Raphson procedure, shifts towards the weakly correlated limit with increasing ring size N, as may be seen from Fig. 4 for the Hubbard Hamiltonian. Approximate values of these critical resonance-integral values β_c^{CCD} are listed in Table VI. The

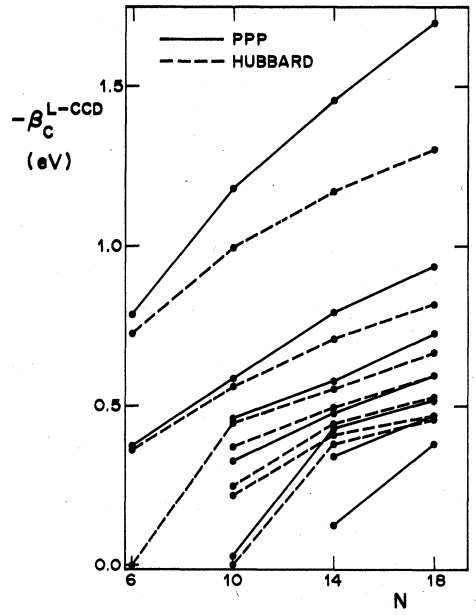

FIG. 2. Dependence of the first few critical resonance-integral values $\beta_c^{\text{L-CCD}}$ (in eV) on the size of the cyclic polyene model, N, for both the PPP (points connected by the solid lines) and the Hubbard (dashed lines) Hamiltonians. (For the first three polyenes all critical values are shown.) For each such critical value, the L-CCD correlation energy has a singularity ($\Delta\epsilon\rightarrow\pm\infty$) (Refs. 32 and 52).

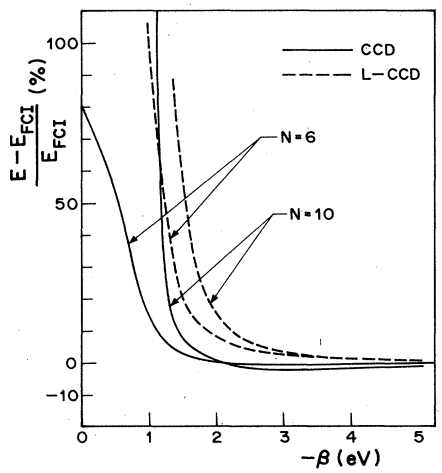

FIG. 3. Percentage error of the L-CCD (dashed lines) and CCD (solid lines) correlation energies (0% for exact full CI energies) as a function of the resonance integral β (in eV) for the first two PPP models ($N=6$ and 10) of the cyclic polyene homologous series C_NH_N. Note that the L-CCD curves pass through a singularity given by the $\beta_c^{\text{L-CCD}}$ values shown in Fig. 2.

TABLE II. Comparison of correlation energies per electron $\Delta\epsilon/N$ (in eV, all signs reversed) obtained with various methods for the PPP Hamiltonian model of C_6H_6 for different coupling constants as measured by the resonance-integral β (in eV) values, ranging from the fully correlated ($\beta=0$) to the weakly correlated ($\beta=-5$ eV) limits. Various CI results are followed by the CC results (the last five columns). The exact result was obtained by using the full CI (Ref. 17). For limited CI approaches (next four columns), D, T, Q, and H indicate that, respectively, doubly, triply, quadruply and hextuply excited configurations were taken into account. The last five columns correspond to various CC approaches: L-CCD and CCD designate the linear and the full CPMET results, D123 and D12 designate CCD approximations with nonlinear diagrams 1,2,3 and 1,2 of Fig. 10(c), respectively, and finally RPA' was obtained considering only the ring-type diagrams 6 of Fig. 10(b) and 1 of Fig. 10(c) [and, of course, the absolute and denominator terms given by diagrams of Fig. 10(a) and diagrams 1 and 2 of Fig. 10(b)]. The percentage errors of these various procedures (0% for FCI) are shown in parentheses. (NC, where present in all tables, signifies that no convergence was obtained.)

$-\beta$	Exact (FCI)	DQH-CI	DTQ-CI	DQ-CI	D-CI	L-CCD	CCD	D123	D12	RPA'
5.0	0.1111	0.1108	0.1111	0.1108	0.1090	0.1121	0.1108	0.1123	0.1147	0.0709
		(0.33)	(0.00)	(0.27)	(1.94)	(−0.85)	(0.29)	(−1.02)	(−3.25)	(36.20)
4.0	0.1395	0.1388	0.1395	0.1389	0.1353	0.1414	0.1390	0.1420	0.1473	0.0813
		(0.49)	(0.01)	(0.45)	(2.98)	(−1.40)	(0.35)	(−1.80)	(−5.58)	(41.70)
3.5	0.1600	0.1592	0.1560	0.1591	0.1539	0.1631	0.1593	0.1641	0.1727	0.0878
		(0.62)	(0.02)	(0.58)	(3.83)	(−1.92)	(0.43)	(−2.57)	(−7.92)	(45.14)
3.0	0.1878	0.1862	0.1877	0.1863	0.1782	0.1930	0.1869	0.1952	0.2109	0.0954
		(0.81)	(0.05)	(0.83)	(5.09)	(−2.80)	(0.45)	(−3.94)	(−12.34)	(49.20)
2.5	0.2273	0.2248	0.2271	0.2247	0.2113	0.2375	0.2265	0.2428	0.2801	0.1044
		(1.09)	(0.08)	(1.13)	(7.03)	(−4.48)	(0.36)	(−6.80)	(−23.22)	(54.06)
2.0	0.2877	0.2835	0.2872	0.2831	0.2585	0.3117	0.2883	0.3292	NC	0.1154
		(1.46)	(0.18)	(1.60)	(10.15)	(−8.35)	(−0.23)	(−14.41)		(59.88)
1.5	0.3884	0.3811	0.3866	0.3796	0.3294	0.4676	0.3996	0.6212		0.1291
		(1.86)	(0.45)	(2.28)	(15.20)	(−20.39)	(−2.88)	(−59.94)		(66.77)
1.0	0.5702	0.5600	0.5631	0.5533	0.4410	1.1556	0.6567	NC		0.1464
		(1.82)	(1.24)	(2.97)	(22.65)	(−102.67)	(−15.17)			(74.32)
0.5	0.8983	0.8919	0.8702	0.8658	0.6190		1.3818			0.1694
		(0.72)	(3.13)	(3.62)	(31.09)		(−53.82)			(81.14)
0.0	1.4403	1.4403	1.4403	1.3580	0.8889		2.5977			0.2014
		(0.00)	(0.00)	(5.71)	(38.28)		(−80.36)			(86.02)

TABLE III. Same as Table II for the PPP Hamiltonian model of $C_{10}H_{10}$ (limited CI results are shown only for the DTQ, DQ, and D configuration selections).

$-\beta$	Exact	DTQ-CI	DQ-CI	D-CI	L-CCD	CCD	D123	D12	RPA′
5.0	0.1270	0.1269	0.1254	0.1204	0.1281	0.1256	0.1285	0.1334	0.0793
		(0.08)	(1.25)	(5.13)	(−0.94)	(1.10)	(−1.24)	(−5.06)	(37.53)
4.0	0.1594	0.1591	0.1564	0.1472	0.1620	0.1570	0.1634	0.1747	0.0905
		(0.20)	(1.90)	(7.68)	(−1.63)	(1.49)	(−2.47)	(−9.58)	(43.22)
3.5	0.1831	0.1825	0.1787	0.1654	0.1874	0.1800	0.1902	0.2113	0.0974
		(0.34)	(2.42)	(9.69)	(−2.35)	(1.71)	(−3.89)	(−15.40)	(46.79)
3.0	0.2154	0.2141	0.2085	0.1884	0.2234	0.2114	0.2304	0.2924	0.1056
		(0.60)	(3.20)	(12.53)	(−3.71)	(1.85)	(−6.94)	(−35.74)	(51.01)
2.5	0.2619	0.2589	0.2504	0.2184	0.2796	0.2579	0.3035	NC	0.1152
		(1.16)	(4.39)	(16.62)	(−6.75)	(1.52)	(−15.87)		(56.03)
2.0	0.3331	0.3252	0.3124	0.2587	0.3846	0.3364	NC		0.1268
		(2.40)	(6.22)	(22.47)	(−15.45)	(−0.98)			(61.95)
1.5	0.4489	0.4266	0.4090	0.3127	0.7122	0.5281			0.1411
		(4.97)	(8.89)	(30.35)	(−58.65)	(−17.64)			(68.57)
1.0	0.6526	0.5801	0.5620	0.3881		4.5335			0.1593
		(11.12)	(13.88)	(40.54)		(−594.63)			(75.60)
0.5	0.9664	0.8021	0.7943	0.4929		9.4630			0.1831
		(17.00)	(17.81)	(48.99)		(−879.23)			(81.05)
0.0	1.4920	1.1213	1.1204	0.6383		13.6222			0.2162
		(24.84)	(24.90)	(57.22)		(−813.04)			(85.51)

TABLE IV. Same as Table III for the Hubbard Hamiltonian model of C_6H_6.

$-\beta$	Exact	DTQ-CI	DQ-CI	D-CI	L-CCD	CCD	D123	D12	RPA′
5.0	0.0843	0.0843	0.0842	0.0832	0.0849	0.0842	0.0849	0.0861	0.0734
		(0.00)	(0.10)	(1.34)	(−0.67)	(0.08)	(−0.72)	(−2.19)	(12.95)
4.0	0.1056	0.1056	0.1055	0.1034	0.1068	0.1055	0.1069	0.1095	0.0891
		(0.01)	(0.17)	(2.07)	(−1.08)	(0.11)	(−1.20)	(−3.61)	(15.65)
3.5	0.1210	0.1210	0.1207	0.1177	0.1227	0.1208	0.1230	0.1270	0.0998
		(0.01)	(0.22)	(2.69)	(−1.45)	(0.13)	(−1.65)	(−4.95)	(17.48)
3.0	0.1415	0.1415	0.1411	0.1364	0.1444	0.1413	0.1450	0.1518	0.1135
		(0.02)	(0.31)	(3.59)	(−2.05)	(0.14)	(−2.42)	(−7.27)	(19.80)
2.5	0.1706	0.1705	0.1698	0.1620	0.1759	0.1704	0.1772	0.1911	0.1317
		(0.05)	(0.46)	(5.05)	(−3.12)	(0.12)	(−3.87)	(−12.01)	(22.83)
2.0	0.2147	0.2145	0.2131	0.1986	0.2263	0.2149	0.2304	0.2711	0.1568
		(0.12)	(0.75)	(7.51)	(−5.40)	(−0.07)	(−7.32)	(−26.24)	(26.96)
1.5	0.2890	0.2880	0.2851	0.2544	0.3232	0.2921	0.3471	NC	0.1944
		(0.34)	(1.33)	(11.94)	(−11.86)	(−1.09)	(−20.13)		(32.73)
1.0	0.4313	0.4268	0.4208	0.3457	0.6413	0.4648	NC		0.2569
		(1.05)	(2.44)	(17.83)	(−48.71)	(−7.78)			(40.42)
0.5	0.7220	0.7004	0.6956	0.5026		1.0449			0.3863
		(3.00)	(3.66)	(30.39)		(−44.71)			(46.51)
0.0	1.25	1.25	1.1805	0.7721		2.1396			1.25
		(0.00)	(5.56)	(38.23)		(−71.17)			(0.00)

TABLE V. Same as Table III for the Hubbard Hamiltonian model of $C_{10}H_{10}$.

$-\beta$	Exact	DTQ-CI	DQ-CI	D-CI	L-CCD	CCD	D123	D12	RPA'
5.0	0.0851	0.0850	0.0848	0.0826	0.0857	0.0849	0.0857	0.0871	0.0737
		(0.04)	(0.28)	(2.93)	(−0.72)	(0.23)	(−0.74)	(−2.42)	(13.34)
4.0	0.1068	0.1067	0.1062	0.1020	0.1080	0.1064	0.1081	0.1111	0.0895
		(0.08)	(0.49)	(4.49)	(−1.16)	(0.35)	(−1.26)	(−4.10)	(16.17)
3.5	0.1224	0.1222	0.1216	0.1153	0.1243	0.1219	0.1247	0.1295	0.1003
		(0.14)	(0.66)	(5.77)	(−1.57)	(0.43)	(−1.77)	(−5.77)	(18.09)
3.0	0.1435	0.1431	0.1421	0.1325	0.1467	0.1427	0.1474	0.1563	0.1140
		(0.25)	(0.97)	(7.65)	(−2.24)	(0.54)	(−2.70)	(−8.90)	(20.57)
2.5	0.1735	0.1726	0.1709	0.1552	0.1796	0.1724	0.1817	0.2029	0.1322
		(0.52)	(1.55)	(10.57)	(−3.51)	(0.63)	(−4.67)	(−16.90)	(23.85)
2.0	0.2197	0.2171	0.2137	0.1862	0.2340	0.2186	0.2435	NC	0.1574
		(1.20)	(2.73)	(15.27)	(−6.49)	(0.49)	(−10.83)		(28.36)
1.5	0.2987	0.2893	0.2828	0.2299	0.3502	0.3049	NC		0.1950
		(3.13)	(5.32)	(23.04)	(−17.24)	(−2.10)			(34.71)
1.0	0.4489	0.4126	0.4020	0.2934	8.9937	1.3666			0.2577
		(8.10)	(10.46)	(34.64)	(−1903.41)	(−204.41)			(42.61)
0.5	0.7380	0.6149	0.6079	0.3874		5.1403			0.3870
		(16.68)	(17.63)	(47.50)		(−596.55)			(47.55)
0.0	1.25	0.9384	0.9367	0.5298		7.8863			1.25
		(24.93)	(25.07)	(57.62)		(−530.90)			(0.00)

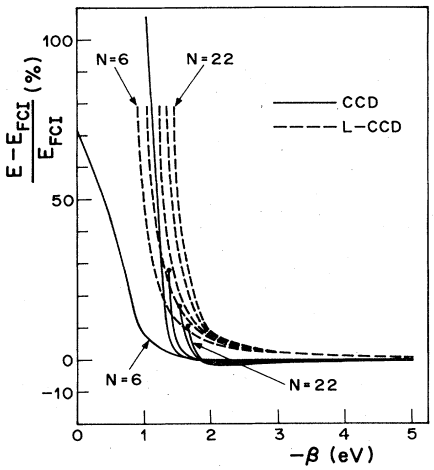

FIG. 4. Same as Fig. 3 for the Hubbard Hamiltonian models of the cyclic polyenes C_NH_N with $N=6$, 10, 14, 18, and 22. [Only the first ($N=6$) and the last ($N=22$) shown dependencies are labeled explicitly, since other curves placed consecutively between the first and last ones can be easily identified.] The CCD curves for $N \geq 14$ terminate at the β_c^{CCD} values (see Table VI).

L-CCD and CCD results for cyclic polyenes with $N=6$–22 in the region of β values, where the solutions exist, are given for both the PPP and the Hubbard Hamiltonian descriptions in Tables II–V, VII, and VIII, and for $N=22$ also in Fig. 5.

Thus, while the singularities in the $\underline{B}$ matrix, which invalidate the L-CCD procedure, are overcome when the nonlinear pair-coupling terms of the CCD are included, for the first two members of the cyclic polyene series, a new kind of singularity seems to appear for larger cycles, which makes the Jacobian of the CCD systems, Eq. (10), singular, thus invalidating the Newton-Raphson procedure. We shall examine the nature of this singular behavior and its remedy in the following sections.

TABLE VI. Critical values β_c^{CCD} of the resonance integral (in eV) defining the critical value of the coupling constant for which the Jacobian of the ground-state CCD equations becomes singular, for both the PPP and the Hubbard Hamiltonian models of cyclic polyenes C_NH_N, $N=4\nu+2$, $\nu=3$–6. (No such singularity occurs for the first two cycles $N=6$ and 10.)

N	14	18	22	26
PPP	−1.75	−2.08	−2.34	−2.55
Hubbard	−1.37	−1.54	−1.66	−1.75

V. SINGULAR BEHAVIOR OF THE CCD APPROACH

We now examine the nature of the singularity which causes the failure of the Newton-Raphson procedure to obtain any solution of the CCD equations below the critical β values listed in Table VI. We mention that the general conditions for the solvability and uniqueness of the CCD equations have been examined earlier.[65] Here we do not attempt to give any general theorems, which is rather difficult for the nonlinear systems, but we simply examine the nature of the singular behavior for the cyclic polyene

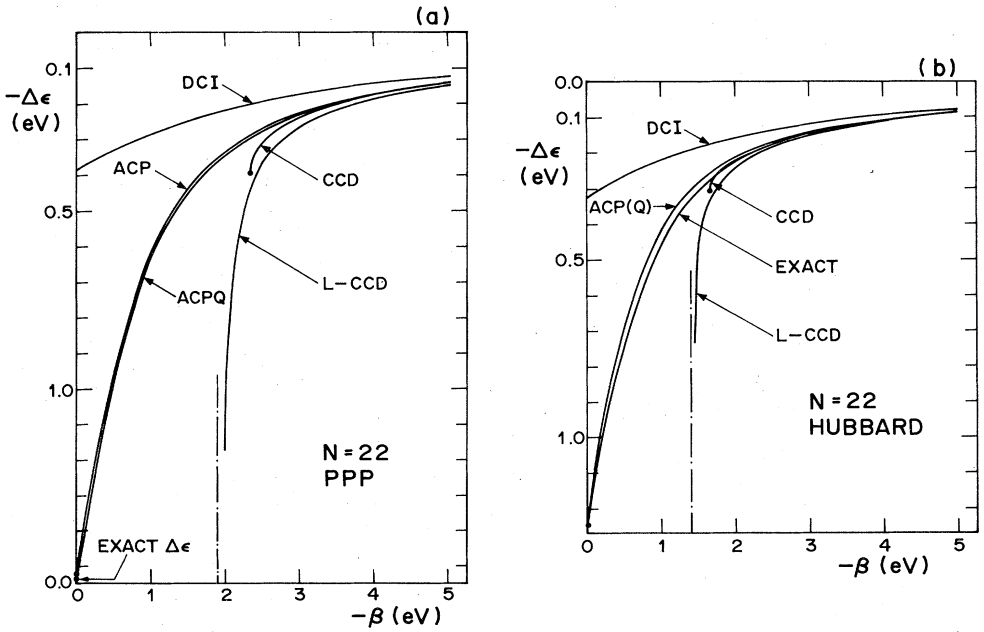

FIG. 5. Total correlation energy $\Delta\epsilon$ (in eV) as a function of the resonance integral β (in eV) for the (a) PPP and (b) Hubbard Hamiltonian models of the cyclic polyene with $N=22$, obtained with L-CCD, CCD, ACP, and ACPQ coupled-cluster approaches. For comparison, a limited CI with doubly excited configurations (D-CI) is also shown. The critical value $\beta_c^{L\text{-}CCD}$ is indicated by the vertical dashed-dotted line representing the asymptote to the L-CCD energy, while the CCD curve ends at β_c^{CCD}. The exact value of $\Delta\epsilon$ corresponding to $\beta=0$ limit is also indicated. For the Hubbard Hamiltonian model, the exact correlation energies (EXACT) were obtained (Ref. 62) by solving Lieb and Wu equations (Ref. 63). Note that the ACP and the ACPQ approximations yield an identical result for the Hubbard Hamiltonian (see the text for details).

TABLE VII. Correlation energies per electron $\Delta\epsilon/N$ (in eV, all signs reversed) obtained with linear (L-CCD) and full (CCD) CPMET approaches, as well as with CI limited to doubly excited configurations (D-CI), for the PPP Hamiltonian model of cyclic polyenes C_NH_N with $N=14$, 18, 22, and 26 for various values of the resonance integral β (in eV). The L-CCD results are shown only for $|\beta| > |\beta_c^{\text{L-CCD}}|$ (i.e., before the first singularity in the $\underline{B}$ matrix occurs); NC designates that no convergence was obtained in solving the CCD equations with the first-order Newton-Raphson procedure.

$N=$		14			18			22			26	
$-\beta$	CCD	L-CCD	D-CI	CCD	L-CCD	D-CI	CCD	L-CCD	D-CI	CCD	L-CCD	D-CI
5.0	0.1329	0.1368	0.1239	0.1370	0.1420	0.1242	0.1395	0.1455	0.1230	0.1411	0.1480	0.1213
4.0	0.1660	0.1734	0.1492	0.1711	0.1806	0.1477	0.1742	0.1857	0.1449	0.1764	0.1898	0.1416
3.0	0.2243	0.2421	0.1865	0.2324	0.2560	0.1811	0.2385	0.2682	0.1751	0.2439	0.2805	0.1693
2.5	0.2766	0.3097	0.2123	0.2920	0.3377	0.2035	0.3112	0.3706	0.1948	NC	0.4196	0.1869
2.0	0.3819	0.4606	0.2450	NC	0.5912	0.2310	NC	1.1340	0.2186			0.2081
1.5	NC	2.9166	0.2873			0.2654			0.2478			0.2335
1.0			0.3422			0.3087			0.2837			0.2643
0.5			0.4142			0.3635			0.3282			0.3019
0.0			0.5091			0.4333			0.3835			0.3479

TABLE VIII. Same as Table VII for the Hubbard Hamiltonian model. In this case the exact correlation energies per electron, as obtained (Ref. 62) by solving the Lieb and Wu equations (Ref. 63), are also shown.

$N=$		14				18				22				26		
$-\beta$	Exact	CCD	L-CCD	D-CI	Exact	CCD	L-CCD	D-CI	Exact	CCD	L-CCD	D-CI	Exact	CCD	L-CCD	D-CI
5.0	0.0853	0.0850	0.0859	0.0815	0.0854	0.0851	0.0861	0.0804	0.0855	0.0851	0.0861	0.0794	0.0855	0.0851	0.0862	0.0783
4.0	0.1071	0.1066	0.1084	0.0999	0.1073	0.1066	0.1086	0.0979	0.1074	0.1067	0.1087	0.0961	0.1075	0.1067	0.1088	0.0943
3.0	0.1442	0.1430	0.1476	0.1281	0.1446	0.1431	0.1480	0.1241	0.1448	0.1431	0.1483	0.1206	0.1450	0.1431	0.1485	0.1174
2.5	0.1747	0.1729	0.1812	0.1483	0.1754	0.1730	0.1821	0.1424	0.1758	0.1730	0.1827	0.1373	0.1761	0.1730	0.1831	0.1329
2.0	0.2220	0.2200	0.2380	0.1750	0.2233	0.2206	0.2408	0.1659	0.2242	0.2210	0.2431	0.1585	0.2248	0.2214	0.2451	0.1522
1.5	0.3032	0.3190	0.3750	0.2108	0.3058	NC	0.4084	0.1966	0.3074	NC	0.4730	0.1855	0.3084	NC	0.7334	0.1764
1.0	0.4555	NC		0.2590	0.4585			0.2371	0.4601			0.2202	0.4610			0.2070
0.5	0.7424			0.3275	0.7442			0.2908	0.7451			0.2651	0.7456			0.2457
0.0	1.25			0.4217	1.25			0.3621	1.25			0.3230	1.25			0.2945

case studied here, where any conclusion made can be verified by the numerical evidence as well.

The resonance integral β occurs only in the diagonal terms of the $\underline{B}$ matrix [arising from the difference of orbital energies, as given by the one-body diagrams 1 and 2 of Fig. 10(b), which corresponds to the MBPT denominator part], so that we can write

$$b_{ij}=b_{ij}^0+\beta\delta_{ij}\tilde{b}_i \ , \tag{27}$$

making the coefficients a_i, b_{ij}^0, $\tilde{b}_i$, and c_{ijk} of the CCD equations (10) β independent. Designating the left-hand side of Eq. (10) by f_i, i.e.,

$$f_i\equiv a_i+\sum_{j=1}^{m} b_{ij}t_j+\sum_{j=1}^{m}\sum_{k=1}^{m} c_{ijk}t_jt_k \ , \tag{28}$$

we can write the CCD equations as

$$f_i(\underline{t})=0 \ , \quad i=1,\ldots,m_T\equiv m \tag{29}$$

where $\underline{t}$ is the row vector with components t_i, $\underline{t}\equiv(t_1,t_2,\ldots,t_m)$.

We have seen in the preceding section that Eq. (29) is unable to provide any reasonably converged solution in the intermediately and strongly correlated regions starting with the $N=14$ ring, even when the solution is very carefully followed from the weakly correlated side. Indeed, we have seen that one can find empirically the critical β value, $\beta=\beta_c^{\mathrm{CCD}}$ (cf. Table VI), beyond which no real solution can be found using either the straightforward zero-order iterative procedure (of the Jacobi type) or the first-order Newton-Raphson procedure.

We shall now show that under certain very plausible assumptions there exists a singluar point $\beta=\beta^0$, beyond which no real solution can be obtained, which is continuous as a function of β from the weakly correlated side. In fact, for $|\beta|<|\beta^0|$ the real solution will become complex, and may not have a simple physical meaning. The numerical evidence will also show us that β^0 is, in fact, identical to β_c^{CCD} determined empirically earlier.

Let us designate the Jacobian of the system (29) for a given value of β by $J(\beta)$,

$$J(\beta)\equiv|J_{ij}(\beta)|\equiv|J_{ij}|=|[\partial\underline{f}_i(\underline{t})]| \ , \tag{30}$$

whose ith row $\partial\underline{f}_i$ has the form

$$\partial\underline{f}_i\equiv\partial\underline{f}_i(\underline{t})\equiv\left|\left|\frac{\partial f_i}{\partial t_j}\right|\right|=\left|\left|b_{ij}+2\sum_{k=1}^{m}c_{ijk}t_k\right|\right| \ , \quad j=1,\ldots,m \ . \tag{31}$$

At the singular point $\beta=\beta^0$ we assume the solution $\underline{t}^0$ to exist,

$$f_i(\underline{t}^0)=0 \ , \tag{32}$$

while the Jacobian (30) vanishes,

$$J(\beta^0)=|\partial\underline{f}_i(\underline{t}^0)|=0 \ . \tag{33}$$

Assuming further that the rank of $J(\beta^0)$ is one less at β^0 than at $|\beta|>|\beta^0|$, it is shown in Appendix B that in the neighborhood of the singularity the Jacobian is proportional to the square root of the resonance-integral difference,

$$\delta J\equiv J(\beta)-J(\beta^0)=J(\beta)\sim|\beta-\beta^0|^{1/2}=|\Delta\beta|^{1/2} \ . \tag{34}$$

Moreover, for $|\beta|<|\beta^0|$ only complex solutions exist.

We have examined this behavior numerically for several cases. The dependence of the square of normalized Jacobian [for each equation of the system (29), the tangent vector given by the ith row, Eq. (31), is normalized to unit

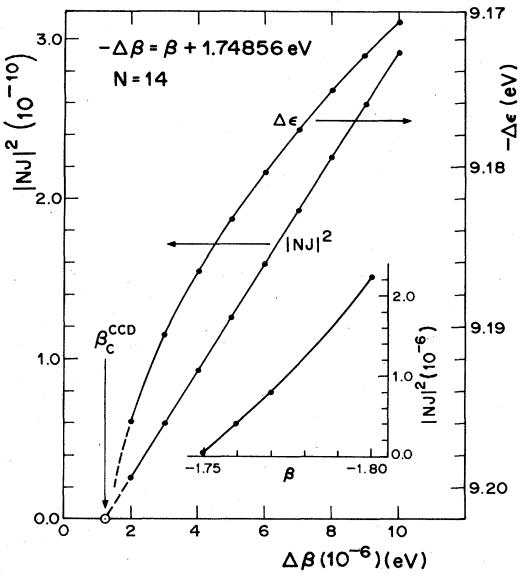

FIG. 6. Square of the normalized Jacobian $|NJ|^2$ of the CCD equations and correlation energy $\Delta\epsilon$ (in eV) as a function of the resonance integral β (in eV) near the critical value β_c^{CCD} for the PPP Hamiltonian model of the cyclic polyene with $N=14$. The inset shows the same dependence of $|NJ|^2$ on β over a wider range of β values. The figure verifies the general behavior near the singular point $\beta=\beta_c^{\mathrm{CCD}}=\beta^0$, as expressed by Eqs. (34) or (B20).

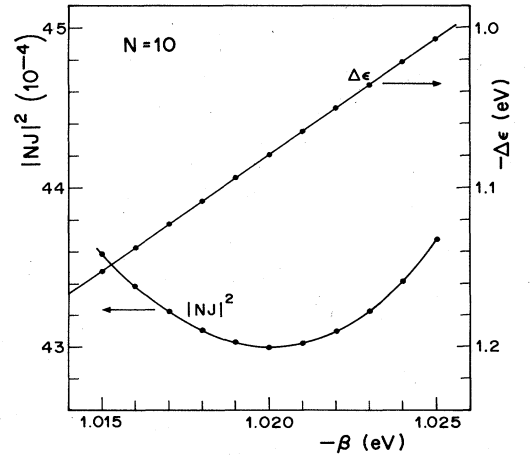

FIG. 7. Dependence of the square of the absolute value of the normalized Jacobian $|NJ|^2$ and of the correlation energy $\Delta\epsilon$ (in eV) on the resonance integral β (in eV) for the Hubbard Hamiltonian model of the cyclic polyene with $N=10$ in the region where $(d\,\Delta\epsilon/d\beta)$ becomes very large.

length], designated by $|NJ|^2$, is plotted as a function of the resonance integral β for the $N=14$ cycle in Fig. 6. The Jacobian obviously vanishes at $\beta_0 \equiv \beta_c^{\mathrm{CCD}} = -1.748\,561\,23$ eV, and in the neighborhood of this point the plot of its square as a function of the resonance integral is remarkably linear, in agreement with Eq. (34). The correlation energy also shows the same $|\Delta\beta|^{1/2}$ dependence in the neighborhood of β^0 (cf. Fig. 6).

In contrast to this behavior, which is characteristic of cyclic polyenes with $N \geq 14$, the Jacobian does not vanish in the entire region of the coupling constant for $N=6$ and 10. The behavior of the normalized Jacobian $|NJ|$ and of the correlation energy $\Delta\epsilon$ as a function of the resonance integral β, in the region where the energy starts its rapid decline (cf. Figs. 3 and 4), is shown for the Hubbard model of the $N=10$ ring in Fig. 7. We see that in this case, even though the normalized Jacobian becomes very small, it never vanishes, while going through a minimum at $\beta \sim -1.02$ eV. Consequently, the ground-state CCD solution can be followed all the way to the fully correlated limit, even though the correlation energies obtained show an enormously large error (up to a factor of 10 at $\beta=0$).

VI. ACCOUNT OF CONNECTED QUADRUPLY EXCITED CLUSTERS

As we mentioned in the Introduction, the ACP (or ACP-D45) approach, [32–34] in which only the hole-pair–factorizing nonlinear diagrams 4 and 5 [Fig. 10(c)] are considered, generally provides correlation energies which are very close to those obtained with the full CCD approach (or CCSD if $T_1 \neq 0$). This is true even in many highly quasidegenerate situations involving either the orbital- or configurational-type quasidegeneracies.[66] In all test calculations,[32,54] where the exact solution is also known, the ACP result lies, in fact, closer to the exact value, even though only slightly closer (except for some highly configurationally quasidegenerate cases where the difference may be of the order of 1–3 mH). It was generally believed that the contributions from the first three nonlinear diagrams [Fig. 10(c), or from the corresponding two Hugenholtz diagrams, e.g., Fig. 5 of Ref. 50] somehow cancel out so that the ACP-D45 approximation yields essentially the same result as the full CCD approach. This cancellation seems to be supported by the calculations in which only the first three nonlinear diagrams of Fig. 10(c) are considered, since this approximation (called linear ACP-D123) yields correlation energies which are very close to the L-CCD or CPMET (L-CPMET) results,[32,33] in which case all nonlinear terms are neglected. Our detailed study of various combinations of the nonlinear-diagram contributions for the Be atom[33] also indicates an approximate additivity of the individual diagram contributions, and, in particular, a mutual cancellation of the D123 contributions. This can be also seen from the D123 results for cyclic polyenes, which we also included in Tables II–V, and which are very close to the L-CCD results (except in the singular region where no convergence of the ACP-D123 approximation is found). This behavior is further amplified if only the first two (RPA with exchange-type) diagrams [Fig. 10(c)] are considered, as may be seen from Tables II–V. (Note that in our D12 approximation, all linear diagrams are considered.) In view of the behavior of the ACP approach just outlined, it would seem of little interest to apply it to the cyclic polyene case. However, we have recently[30] shown that the ACP approach is, in fact, very close to the ACPQ approach, which accounts approximately for the connected $\hat{T}_4$ clusters. It is precisely the $\hat{T}_4$ component which becomes important in the highly correlated region, as we have shown by an explicit cluster analysis of the exact wave function in the $N=6$ and 10 cases.[17] As one approaches the fully correlated limit, the basic assumption of the CPMET, namely that $\frac{1}{2}\hat{T}_2^2 \gg \hat{T}_4$, breaks down, as it does generally in quasidegenerate situations. It is thus interesting to test both the ACP and the proper ACPQ approaches in the highly degenerate situations represented by the strongly correlated limit of the cyclic polyene models. These results are presented in Tables IX and X, together with the exact results whenever available (see also Fig. 5 for the $N=22$ case).

We note immediately that the ACP approximation already provides excellent correlation energies over the entire region of the coupling constant. In fact, for the Hubbard Hamiltonian, both the ACP and ACPQ approaches yield the exact result in the fully correlated limit ($\beta=0$), while for the more demanding PPP Hamiltonian, this is only true for the ACPQ approach, even though the ACP result is still very close to the exact result in the $\beta=0$ limit. Indeed, both approaches yield amazingly good correlation energies, particularly in view of the highly singular behavior of both the L-CCD and full CCD approaches. The plot of the correlation energy as a function of the resonance integral β, obtained with various approaches for both the PPP and the Hubbard models of the $N=22$ cyclic polyene, is shown in Figs. 5(a) and 5(b), respectively. In the Hubbard case, the ACP and ACPQ approaches yield identical results (see Discussion), while only a very minute difference can be discerned in the PPP case [Fig. 5(a)]. Finally, in contrast to the full CCD approach, not even slightest convergency difficulties are encountered with either the ACP or ACPQ approaches.

VII. DISCUSSION

The cyclic polyene model, and the metalliclike systems in general, represent one of the most challenging correlation problems, particularly in the strongly correlated region of the coupling constant. The high orbital and configuration degeneracy[61] requires that the high-order excitations are properly taken into account, and the importance of higher-than-triexcited connected clusters causes the commonly used pair approximations, including the full CCD approach, to break down. Likewise, the approaches which are so successful for finite systems are plagued with fundamental difficulties when applied to these systems, be it the size extensivity problem for the limited CI approaches or convergency problems for the finite-order MBPT. Yet this model plays the role of a simple prototype for the metalliclike quasi-one-dimensional systems, not unlike the role played by the electron-gas model for three-dimensional systems. How-

TABLE IX. Correlation energies per electron $\Delta\epsilon/N$ (in eV, all signs reversed) obtained with the ACP and the ACPQ approximations (see the text) for the PPP Hamiltonian model of cyclic polyenes C_NH_N with $N=6$, 10, 14, 18, and 22, for various values of the resonance integral β (in eV). The percentage error is enclosed in parentheses wherever the exact solution is available.

$N=$	6		10		14		18		22	
$-\beta$	ACP	ACPQ	ACP	ACPQ	ACP	ACPQ	ACP	ACPQ	ACP	ACPQ
5.0	0.1106	0.1107	0.1253	0.1257	0.1326	0.1334	0.1366	0.1378	0.1391	0.1406
	(0.44)	(0.33)	(1.31)	(0.96)						
4.0	0.1385	0.1387	0.1562	0.1569	0.1648	0.1661	0.1695	0.1713	0.1723	0.1745
	(0.71)	(0.59)	(2.05)	(1.57)						
3.0	0.1853	0.1857	0.2078	0.2093	0.2185	0.2209	0.2242	0.2273	0.2276	0.2311
	(1.29)	(1.10)	(3.52)	(2.85)						
2.5	0.2231	0.2238	0.2494	0.2515	0.2616	0.2649	0.2680	0.2720	0.2717	0.2763
	(1.84)	(1.55)	(4.77)	(3.97)						
2.0	0.2799	0.2811	0.3117	0.3149	0.3259	0.3305	0.3331	0.3385	0.3371	0.3429
	(2.69)	(2.30)	(6.44)	(5.48)						
1.5	0.3732	0.3756	0.4129	0.4180	0.4295	0.4360	0.4375	0.4444	0.4416	0.4488
	(3.90)	(3.31)	(8.03)	(6.89)						
1.0	0.5429	0.5482	0.5924	0.6004	0.6114	0.6198	0.6199	0.6281	0.6241	0.6320
	(4.79)	(3.87)	(9.23)	(8.00)						
0.5	0.8681	0.8797	0.9256	0.9370	0.9483	0.9583	0.9595	0.9683	0.9657	0.9736
	(3.36)	(2.07)	(4.22)	(3.04)						
0.0	1.4207	1.4403	1.4770	1.4920	1.5032	1.5149	1.5176	1.5271	1.5263	1.5343
	(1.36)	(0.00)	(1.00)	(0.00)	(0.77)	(0.00)	(0.62)	(0.00)	(0.52)	(0.00)

TABLE X. Same as Table IX for the Hubbard Hamiltonian model. (Note that in this case both the ACP and ACPQ approximations yield the same result.)

N	6	10	14	18	22
$-\beta$	ACP,ACPQ	ACP,ACPQ	ACP,ACPQ	ACP,ACPQ	ACP,ACPQ
5.0	0.0842	0.0849	0.0851	0.0851	0.0852
	(0.12)	(0.24)	(0.30)	(0.35)	(0.38)
4.0	0.1054	0.1063	0.1066	0.1066	0.1067
	(0.21)	(0.41)	(0.53)	(0.61)	(0.66)
3.0	0.1409	0.1423	0.1426	0.1428	0.1428
	(0.43)	(0.83)	(1.09)	(1.28)	(1.41)
2.5	0.1695	0.1713	0.1717	0.1718	0.1718
	(0.66)	(1.31)	(1.73)	(2.04)	(2.27)
2.0	0.2124	0.2149	0.2154	0.2155	0.2154
	(1.09)	(2.20)	(2.96)	(3.50)	(3.91)
1.5	0.2834	0.2871	0.2876	0.2874	0.2871
	(1.92)	(3.86)	(5.15)	(6.02)	(6.60)
1.0	0.4177	0.4228	0.4224	0.4211	0.4200
	(3.14)	(5.81)	(7.28)	(8.15)	(8.72)
0.5	0.7039	0.7084	0.7066	0.7045	0.7027
	(2.51)	(4.01)	(4.82)	(5.33)	(5.69)
0.0	1.25	1.25	1.25	1.25	1.25
	(0.00)	(0.00)	(0.00)	(0.00)	(0.00)

ever, the strength and character of the interelectron correlations is rather unique in the cyclic polyene models due to their low dimensionality, with electrons colliding "head-on" and having no option to avoid one another, even though this model shares many of the interesting properties of the three-dimensional electron-gas model which arise from the long-range nature of Coulomb forces whose infinite range of interaction gives the correlation effects such a prominence in these systems. It should be noted, however, that even for the Hubbard Hamiltonian models, when only on-site interactions are permitted, very much the same type of correlation problem arises. Consequently, the degeneracies encountered in the strongly correlated limit of these models have a decisive role to play.

In order to better realize the nature of the correlation problem at hand, we recall[17] some of the CI results for the first two members ($N=6$ and 10) of the cyclic polyene homologous series, keeping in mind that the intricacies involved will be only amplified with increasing N. In the weakly correlated limit, and even for the intermediate values of the coupling constant corresponding to physical densities ($\beta\sim-2.5$ eV), the CI limited to biexcited configurations provides a very good approximation (cf. Tables II–V). However, in the fully correlated limit, the error in the correlation energy is 40% and 60% for $N=6$ and 10, respectively. It is well known that, in fact, for the $N\rightarrow\infty$ case, the biexcited CI wave function will have a zero overlap with the exact wave function, and the correlation energy per particle $\Delta\epsilon/N$ will tend to zero as $1/\sqrt{N}$. This tendency is already clearly evident from the $N=22$ results of Figs. 5(a) and 5(b), and particularly from the $\Delta\epsilon/N$ plots in Figs. 9. The role of the triexcited configurations being relatively minor (at most 2% of the correlation energy over the entire range of the coupling constant; see, e.g., the third column in Table II), the next important contribution is due to the tetraexcited configurations (see also Refs. 41 and 67). For the $N=6$ cycle, proceeding up to the quadruple CI yields very accurate correlation energies over the entire range of the coupling constant (the largest error is $\sim3\%$ for $\beta\sim-0.5$ eV) and the exact result in the fully correlated limit for both the Hubbard and the PPP Hamiltonians. However, already for the $N=10$ cycle, the error of the limited CI including biexcited through tetraexcited configurations monotonically increases as the fully correlated limit is approached. While still providing an excellent result (0.5% error for the Hubbard model and 1.2% error for the PPP Hamiltonian) for the spectroscopic value of the coupling constant ($\beta\sim-2.5$ eV), an error of almost 25% results in the fully correlated limit.[17] This error is clearly due to the higher-than-tetraexcited contributions. Since the odd-number-of-times–excited contributions can be generally expected to play a lesser role in view of the cluster structure of the wave function and the prominence of pair correlations,[41,67] this 25% error must be primarily due to the neglect of hextuply excited configurations. Since there is only one such configuration in the $N=6$ case which, moreover, becomes degenerate with the ground state in the fully correlated limit, we can understand the above-stated behavior of the quadruply excited CI for this system.

Obviously, this situation, with respect to the importance of highly excited configurations, will become more and more aggravated as N increases. The CC approach could obviously remedy this situation, assuming that only the *disconnected,* highly excited clusters play the role. Unfortunately, in view of the degeneracies present in the fully correlated limit, this cannot be the case. Our cluster analysis of the exact full CI wave functions for the first two cycles[17] clearly indicates the increasing importance of the *connected,* quadruply excited component $\hat{T}_4$ as the highly correlated regime is approached (cf. Figs. 8–11 of Ref. 17). Moreover, in view of the high symmetry of

these systems, a new phenomenon enters into play (for the first time in the $N=10$ ring), namely the fact that certain quadruply excited configurations cannot be obtained as products of zero-quasimomentum biexcitations. Thus for 24 (from over 500, alternancy symmetry being ignored) quadruply excited configurations of $C_{10}H_{10}$, the sole contribution is from $\hat{T}_4$, while the $\frac{1}{2}\hat{T}_2^2$ contribution vanishes altogether [see Eqs. (31) and (32) of Ref. 17, and the following discussion]. The number of configurations of this type will rise faster, relative to the total number of quadruples, than the number of those which can be associated with the disconnected $\frac{1}{2}\hat{T}_2^2$ component. Indeed, we have seen in Sec. III that the requirement of zero overall quasimomentum for the totally symmetric ground state reduces the n^{2p} dependence for the number of p-times-excited configurations to n^{2p-1}, the other symmetries modifying only the n-independent multiplicative factor ($n^3/6$ for the biexcited configurations when all the symmetries are accounted for). Thus we immediately see that the number of zero-quasimomentum tetraexcited configurations will vary as n^7 when $n=\frac{1}{2}N\to\infty$, while the number of tetraexcited configurations of the disconnected $\frac{1}{2}\hat{T}_2^2$ type will vary only as $(n^3)^2=n^6$, ignoring all numerical factors. Clearly, the extra $n=n^7/n^6$ dependence arises due to the configurations of the type mentioned above for the $N=10$ case, for which the $\frac{1}{2}\hat{T}_2^2$ contribution vanishes altogether. Even though the number of connected tetraexcited clusters which cannot be represented as products of zero-quasimomentum pair clusters will dominate in the quadruply excited manifold as $N\to\infty$, as we have just shown, the role played by these clusters in the determination of the exact correlation energy is not entirely clear and deserves further investigation.

Now, in the CC formalism, the energy is determined solely by the pair clusters (and, of course, the T_1 clusters, if present), while the CCD equations determining these clusters can involve, at most, the $\hat{T}_4$ clusters, since the electronic Hamiltonian can contain, at most, two-body terms. Thus, if we could somehow determine the $\hat{T}_4$ contribution (in the usual CCD approach we neglect them), we could use them to correct the pair equations and obtain, in principle, the exact result. In this way the contributions from all higher excited configurations, say hextuples, would be also automatically accounted for. It is, of course, computationally hopeless to consider the quadruples within the CC formalism, so we must rely on some independent estimate for $\hat{T}_4$. Obviously, if we approximate $\hat{T}_4$, only approximate results can be obtained.

In our recent paper[30] we showed how the $\hat{T}_4$ contribution can be estimated from the unrestricted Hartree-Fock (UHF), or some of its projected versions like the PHF (projected HF) or the AMO (alternant-molecular-orbital) wave functions. By using a general form of such wave functions, we have succeeded in taking into account the $\hat{T}_4$ contribution in a way which only simply modifies the CCD approach. There is, of course, the possibility of actually calculating the correction terms for each pair equation of the CCD approach directly from the UHF, PHF, or AMO wave functions. Such a computational procedure is not very demanding and will be further explored. However, we have also shown that if we *assume* that the UHF- or PHF-type wave function is exact (which, of course, will be true in only very special cases), this procedure will simply modify the CCD equations. This modification essentially results in the ACP approach, in which only the nonlinear diagrams 4 and 5 [Fig. 10(c)] are considered, as already mentioned. The modified ACPQ equations are thus identical to the ACP equations, except for an extra factor of 9 for diagram 5 [Fig. 10(c)] contribution in equations which correspond to the projection on the biexcited states with triplet intermediate spin coupling of pp and hh pairs.

It is well known that the UHF approach, as well as its various projected versions, provides the exact correlation energy in the fully correlated limit (cf., e.g., Refs. 18(a) and 68) of the cyclic polyene systems. Consequently, it is not surprising that the ACPQ approach also yields the exact correlation energy in this limit. In fact, the ACP approach already yields excellent results for the PPP Hamiltonian and the exact result for the Hubbard Hamiltonian. This fact is related to the simple structure of the latter, Eq. (14), which makes the molecular two-electron integrals $K(k)$, Eq. (20), independent of the quasimomentum transfer k, since $K(k)=N^{-1}\gamma_{00}$ in the Hubbard case. In view of the antisymmetric property of the triplet coupled pair clusters [cf. Eqs. (30) and (31) of Ref. 50] the contribution of diagram 5 [Fig. 10(c); see the last term of Eq. (A5)] vanishes when $\tilde{S}=1$, since the two-electron integral is constant. Thus, the exact factor of 9 multiplies, in this case, the zero contribution, thus making no difference between the ACP and ACPQ results in the Hubbard case. It should also be mentioned here that the exact ground state, in fact, becomes degenerate in the fully correlated limit, and the UHF procedure, while yielding the exact energy, gives a wave function which is a linear combination of the degenerate state which would be obtained by an analytic continuation of the ground-state wave function for nonzero β values. This fact, however, does not seem to impede in any way the basic assumptions of the ACPQ approach.

The UHF result for the correlation energy rapidly deteriorates as we move away from the fully correlated limit, yielding zero correlation energy once the critical coupling constant for the triplet instability[21,69] is reached. If the UHF wave function were indeed used to compute the corrections to pair equations, the same abrupt behavior could be expected at the critical β value associated with the triplet (nonsinglet) instability. Of course, this behavior would be smoothed out by using projected procedures (with projection done prior to the optimization), such as the AMO method, and we are currently investigating this possibility. It is, however, most satisfactory that a simple modification of the CCD or, in fact, the ACP equations, which results in the ACPQ approach, is capable of smoothly correcting for the connected $\hat{T}_4$ contribution and providing such remarkable results over the entire region of the coupling constant.

These results also clearly demonstrate how the $\hat{T}_4$ component is essential, so that any attempt to correct for the correlation error in the strongly correlated region of the one-dimensional metalliclike systems (since our cyclic po-

lyene model can be regarded as a model of a linear metal with Born—von Kármán boundary conditions), solely on the basis of the coupled pair (i.e., CCD) approaches, must necessarily fail. In this regard it is remarkable that the pair-cluster approximation (designated SUB2 by Bishop and Lührman[29]), or, in fact, the RPA, which only considers the ring-type diagrams [i.e., diagram 6 of Fig. 10(b) and diagram 1 of Fig. 10(c) considered as Goldstone diagrams], can provide such good results for the three-dimensional electron gas (where the RPA becomes exact in the high-density limit). This undoubtedly reflects on the severity of the correlation problem in the one-dimensional gas analog (except for the discrete rather than continuous positive background) treated in this paper, as stated earlier. In fact, the RPA-type approximation, designated RPA', which results when diagram 6 of Fig. 10(b) and the nonlinear diagram 1 of Fig. 10(c) [and, of course, the absolute-term diagram of Fig. 10(a) and the "denominator" terms given by diagrams 1 and 2 of Fig. 10(b)], are considered [or the so-called RPA with exchange when diagram 5 of Fig. 10(b) and diagram 2 of Fig. 10(c) are also taken into account], yields rather poor results in the one-dimensional case as the data in Tables II—V attest. (Note that even when considering only the first nonlinear term [diagram 1 of Fig. 10(c)], certain exchange terms are automatically included in view of the spin-adapted form we are using.)

Interestingly enough, the RPA' results show a very different behavior for the PPP and the Hubbard Hamiltonians, as graphically illustrated in Fig. 8(a) for the smallest ring, $N=6$. Thus, while in the PPP case a fast convergence is found, when solving the RPA' equations using the Newton-Raphson procedure, over the entire range of the coupling constant with the percentage error in the correlation energy monotonically increasing to almost 90% as the fully correlated limit is approached [Fig. 8(a)], we find a very poor convergence below $|\beta| \sim 0.5$ eV and a nonmonotonic correlation error dependence for the Hubbard Hamiltonian model. Nevertheless, using a very small step in lowering the resonance-integral $|\beta|$ value, we can continue the RPA' solution all the way to the $\beta=0$ limit in the Hubbard Hamiltonian case as well. However, the energy error passes, in this case, through the maximum at about $\beta \approx -0.5$ eV, and the exact solution is obtained in the fully correlated limit. An examination of the corresponding Jacobian shows a singular behavior at $\beta=0$, with the normalized Jacobian approaching zero as $|NJ| \sim |\beta|^{3/2}$ and the correlation energy approaching the exact value at $\beta=0$ ($\Delta\epsilon/N=-1.25$ eV) as $|\beta|^{1/2}$ [Fig. 8(b)]. The behavior of the Jacobian suggests that at $\beta=0$ its rank is reduced from $m=7$ to $m=4$, i.e., by three units, thus yielding the $|\beta|^{3/2}$ dependence. An analogous behavior is found for $N=10$ Hubbard Hamiltonian case, but the rank reduction at $\beta=0$ is even larger in this case, while the energy again shows square-root dependence on $|\beta|$. Needless to say, no singular behavior is found for the PPP Hamiltonian models in either case.

We finally note a rapid "convergence" of the finite-cycle results as N is increased, which was also observed in a number of instances earlier.[18,20–22] To obtain a better

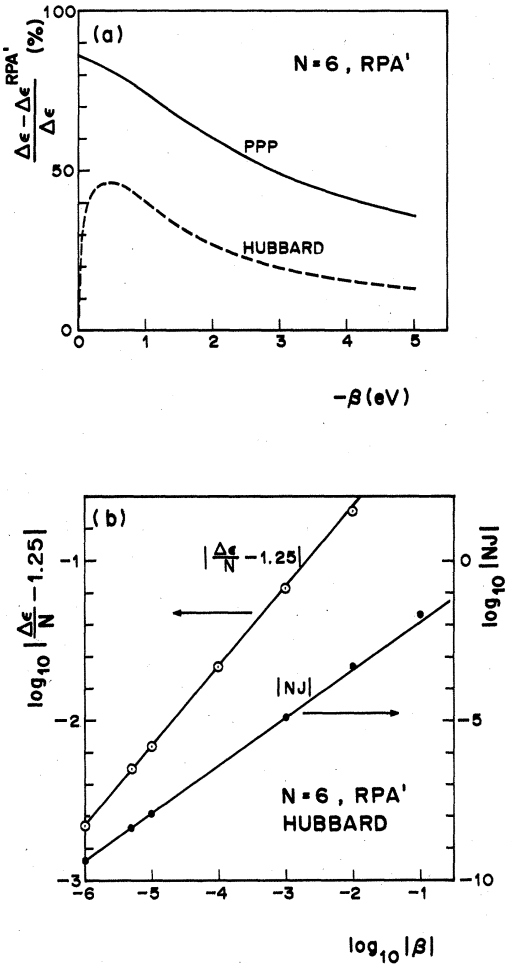

FIG. 8. (a) Dependence of the percentage error in the correlation energy (0% for exact full CI energy) of the RPA' as a function of the resonance integral β (in eV) for both the PPP and the Hubbard Hamiltonian C_6H_6 models. (b) Dependence of the normalized Jacobian $|NJ|$ and of the correlation energy per electron difference ($\Delta\epsilon/N-1.25$) (in eV) on the resonance integral β (in eV) for the Hubbard Hamiltonian C_6H_6 model in the vicinity of the fully correlated limit ($\beta=0$). Note that the $\log_{10}$ scale is used throughout. The slope of the straight lines shows the $|NJ| \sim |\beta|^{3/2}$ and $|\Delta\epsilon/N-1.25| \sim |\beta|^{1/2}$ dependence as $\beta \to 0$.

idea of how the approximations employed in this paper will fare when $N \to \infty$, in Fig. 9 we have plotted the correlation energy per particle $\Delta\epsilon/N$ as a function of the polyene size N (or ν) for the four typical values of the resonance integral ($\beta=0$, -1, -2.5, and -5 eV). We present these results in graphical form only for the Hubbard model, in which case the exact result can be obtained by solving Lieb and Wu equations for any N.[63] (Recall, however, that it is only the correlation energy which is provided by Bethe's ansatz, so that we have no information about the corresponding wave functions.) In these plots (Fig. 9) we also include the biexcited CI (D-CI) result, which clearly shows the size inconsistency of this ap-

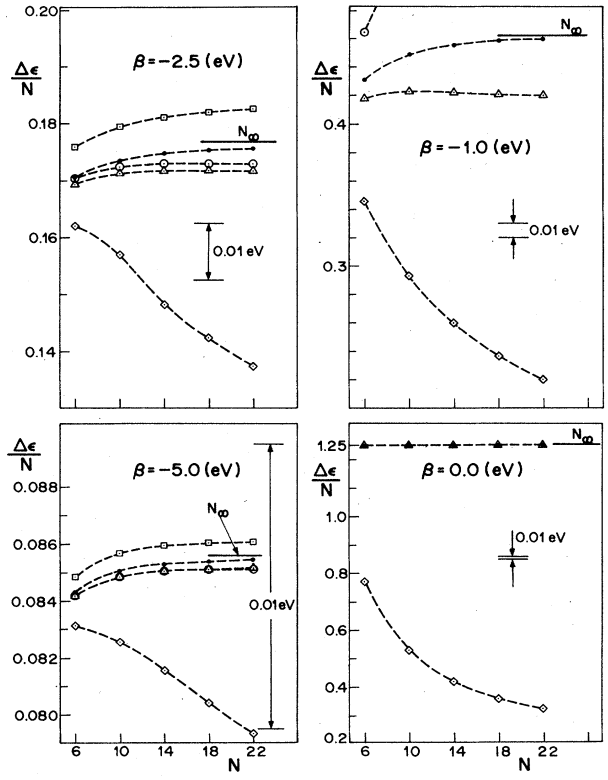

FIG. 9. Correlation energy per electron $\Delta\epsilon/N$ (in eV) as a function of the chain size, as given by the site number N, for the Hubbard model of cyclic polyenes C_NH_N, $N=4\nu+2$, $\nu=1,2,\ldots,5$, for the four typical values of the resonance integral β ($\beta=0$, -1, -2.5, and -5 eV). Here, ● designates the exact energy obtained by solving the Lieb and Wu equations (Ref. 63), △ represents the ACP or ACPQ energies, and □ and ⊙ represent the L-CCD and CCD energies, respectively, wherever available. For comparison, the size-inconsistent D-CI energies (CI limited to doubly excited configurations) is also shown by ◇. The solid horizontal lines indicate the limiting exact values for the infinite chain (Ref. 63). Note that a different energy scale is used for each value of β; for quick orientation the vertical segment on the right-hand side of each figure indicates 0.01 eV.

proach: The correlation energy yielded by this method will, in fact, approach zero as $1/\sqrt{N}$ when $N\to\infty$. On the other hand, all the CC approaches provide a rather quick "convergency" toward the $N\to\infty$ limit in view of their size-extensive behavior. In the strongly correlated region (cf. Fig. 9, $\beta=-1$ eV) the $\Delta\epsilon/N$ dependence on N is not monotonic, passing through the maximum at $N=10$. However, the "saturation" with N is always faster for the ACPQ or ACP correlation energies than for the exact energy (cf. Fig. 9), thus causing the percentage errors given in Table X for the Hubbard Hamiltonian to slightly increase with N. These errors stay below 10% over the entire range of the coupling constant, and in view of the similar behavior of the PPP and Hubbard Hamiltonian correlation energies observed for the $N=6$ and 10 rings, we can hope that the ACPQ correlation energies for the PPP Hamiltonian (Table IX) are also smaller than the exact ones by, at most, about 10%.

To conclude, we shall briefly compare the results presented here with those obtained earlier. We have seen that while the UHF yields the exact correlation energy in the fully correlated limit, it gives zero correlation energy for resonance integrals which are larger in absolute value than the triplet-instability critical β value.[18,21,69] Subsequent projection onto the singlet manifold makes the correlation-energy dependence on the coupling constant even more pathological without significantly improving it.[70] The one-parameter AMO approximation also gives the exact energy for $\beta=0$ and gradually deteriorates as the weakly correlated limit is approached. This deterioration is rather slow for small cycles [still yielding about 70% of the correlation energy in the weakly correlated limit for $N=6$; cf. Fig. 3 of Ref. 18(c)], but it increases rapidly with N [thus yielding less than 50% of the correlation energy when $\beta\to-\infty$ already for the $N=10$ ring; cf. Figs. 4 and 5 of Ref. 18(c)]. The multiparameter AMO results can be expected to be much better; however, the method used to obtain them is rather difficult to implement[57] and becomes very costly, as the number of nonlinear parameters which must be optimized is increased with N. Nevertheless, this method is worthy of further investigation (cf. also Ref. 27), and new ways of obtaining the multiparameter AMO wave functions should be explored (cf., e.g., Ref 71). The finite, as well as some infinite-order (e.g., standard CCD or CPMET), approaches also suffer many shortcomings. Primarily, they pose serious convergency problems as the strongly correlated limit is approached. For finite cycles the radius of convergence of the standard perturbation theory based either on the IPM of the weakly correlated limit (with Hückel or HF Hamiltonians as the unperturbed Hamiltonian) or the strongly correlated limit (with one electron part of the Hamiltonian considered as a perturbation) can be determined.[72] These radii monotonically shift toward their respective limits, thus increasing the divergency gap.[72] For extended chains, the standard perturbation theory based on the weakly correlated limit (i.e., with the Hartree-Fock Hamiltonian as H_0) diverges for all coupling constants,[73] even though the perturbation energy passes through a minimum as a function of the perturbation-theory order (cf. Fig. 9 or Ref. 19), which approximates rather well the true correlation energy (cf. Fig. 10 of Ref. 19). However, already for $\beta=-1$ eV the result obtained in this way is rather poor ($\sim$20% error), and it further rapidly deteriorates as the $\beta=0$ limit is approached.

In view of this behavior of both variational and perturbative approaches, the results afforded by the ACPQ (or, in fact, the ACP) approach are truly remarkable. Moreover, keeping in mind the highly singular behavior of both the L-CCD and the full CCD approaches in the strongly correlated region, it is perhaps even more remarkable that these results are achieved by effectively implementing certain cancellations in the infinite-order MBPT, as approximated and summed by the CCD approach, the result of which is a relatively simpler ACPQ approximation.

ACKNOWLEDGMENTS

This work was supported by a Natural Sciences and Engineering Research Council of Canada Grant-in-Aid for Research (J.P.), which is hereby gratefully acknowledged. We would also like to express our gratitude to Professor J. Čížek for useful discussions, and to Mr. Tom Fairgrieve for help with some computations. One of us (M.T.) would like to express his thanks to the Department of Applied Mathematics of the University of Waterloo, and, in particular, to Professor Paldus and Professor Čížek, for their hospitality during his stay.

APPENDIX A: EXPLICIT FORM OF THE ORTHOGONALLY-SPIN-ADAPTED CCD EQUATIONS

The explicit form of the orthogonally-spin-adapted CCD equations[50] is most simply obtained by exploiting the time-independent diagrammatic technique,[31–46] together with graphical methods of spin algebras.[51] The relevant orbital diagrams (cf. Fig. 3 of Ref. 50) are shown in Fig. 10, where we use Goldstone diagrams to represent one- and two-particle interaction vertices and the Brandow form (one Goldstone representative for each Hugenholtz diagram) to represent pair-cluster vertices. With the latter we associate unnormalized $\hat{\tau}_2$ matrix elements, which we designate as

$$[i,j;k,l]_S := \langle a^i,a^j \mid \hat{\tau}_2 \mid a_k,a_l \rangle_S = [(1+\delta_{a^i a^j})(1+\delta_{a_k a_l})]^{1/2} \langle a^i,a^j \mid \hat{t}_2 \mid a_k,a_l \rangle_S \ , \tag{A1}$$

in order to simplify our expressions (note that the bra part always contains particle labels and the ket part the hole labels). In the one- and two-electron integrals, $\langle a \mid \hat{f} \mid b \rangle$ and $\langle a,b \mid \hat{v} \mid c,d \rangle$, which are associated with one- and two-particle interaction vertices, respectively, we distinguish the hole and particle states by simple and double primes. Thus, e.g., $\langle a^1,a^2 \mid \hat{v} \mid a_1,a_2 \rangle = \langle 1'',2'' \mid \hat{v} \mid 1',2' \rangle$, while for $\hat{\tau}_2$ elements we simply write $\langle a^1,a^2 \mid \hat{\tau}_2 \mid a_1,a_2 \rangle_S = [1,2;1,2]_S$.

The diagrams of Figs. 10(a), 10(b), and 10(c) contain zero, one, and two pair vertices, and yield, respectively, the absolute ($r=0$), linear ($r=1$), and bilinear ($r=2$) terms $\Lambda^{(r)}$ of the CCD equations, Eq. (9), $\kappa=2$,

$$\sum_{r=0}^{2} \Lambda^{(r)}(1'',2'';1',2';\tilde{S}) = 0 \ , \tag{A2}$$

labeled by the configurations

$$\left| \begin{matrix} 1'' & 2'' \\ 1' & 2' \end{matrix} \right\rangle_{\tilde{S}} = \left| \Phi_i^{(2)} \right\rangle \ .$$

These terms, Eq. (A2), have the following explicit form:[30]

$$\Lambda^{(0)}(1'',2'';1',2';\tilde{S}) = -[\tilde{S}]^{1/2} \{ \langle 1'',2'' \mid \hat{v} \mid 2',1' \rangle + (-1)^{\tilde{S}} \langle 1'',2'' \mid \hat{v} \mid 1',2' \rangle \} \ , \tag{A3}$$

$$\begin{aligned} \Lambda^{(1)}(1'',2'';1',2';\tilde{S}) = & \sum_{\kappa=1}^{2} \left\{ \sum_{3''} \langle \kappa'' \mid \hat{f} \mid 3'' \rangle [3,\bar{\kappa};\kappa,\bar{\kappa}]_{\tilde{S}} - \sum_{3'} \langle 3' \mid \hat{f} \mid \kappa' \rangle [\kappa,\bar{\kappa};3,\bar{\kappa}]_{\tilde{S}} \right\} \\ & + \sum_{3'',4''} \langle 1'',2'' \mid \hat{v} \mid 3'',4'' \rangle [3,4;1,2]_{\tilde{S}} + \sum_{3',4'} \langle 3',4' \mid \hat{v} \mid 1',2' \rangle [1,2;3,4]_{\tilde{S}} \\ & + \sum_{\kappa,\lambda=1}^{2} (-1)^{(\kappa+\lambda)\tilde{S}} \sum_{3'',3'} \sum_{S=0}^{1} \{ \tfrac{1}{2} ([S][\tilde{S}])^{1/2} \langle \kappa'',3' \mid \hat{v} \mid \bar{\lambda}',3'' \rangle - \delta_{\tilde{S},S} \langle \kappa'',3' \mid \hat{v} \mid 3'',\bar{\lambda}' \rangle \} [3,\bar{\kappa};\lambda,3]_S , \end{aligned} \tag{A4}$$

$$\begin{aligned} \Lambda^{(2)}(1'',2'';1',2';\tilde{S}) = & \tfrac{1}{4} [\tilde{S}]^{1/2} \sum_{\kappa=1}^{2} (-1)^{\kappa\tilde{S}} \sum_{S,S'=0}^{1} (-1)^{S+S'} ([S]\cdot[S'])^{1/2} \\ & \times \sum_{3',4',3'',4''} [F(\tilde{S}+S+S') \langle 3',4' \mid \hat{v} \mid 4'',3'' \rangle \\ & - \langle 3',4' \mid \hat{v} \mid 3'',4'' \rangle] [1,3;\kappa,3]_S [2,4;\bar{\kappa},4]_{S'} \\ & + \tfrac{1}{2} \sum_{\kappa=1}^{2} (-1)^{\kappa\tilde{S}} \sum_{S=0}^{1} [S]^{1/2} \sum_{3',4',3'',4''} \langle 3',4' \mid \hat{v} \mid 3'',4'' \rangle ([4,\kappa;1,2]_{\tilde{S}} [\bar{\kappa},3;3,4]_S \\ & + [1,2;\bar{\kappa},4]_{\tilde{S}} [3,4;\kappa,3]_S) - (-1)^{\tilde{S}} \tfrac{1}{2} [\tilde{S}]^{-1/2} \sum_{3',4',3'',4''} \langle 3',4' \mid \hat{v} \mid 3'',4'' \rangle [1,2;3,4]_{\tilde{S}} [3,4;1,2]_{\tilde{S}} \ , \end{aligned} \tag{A5}$$

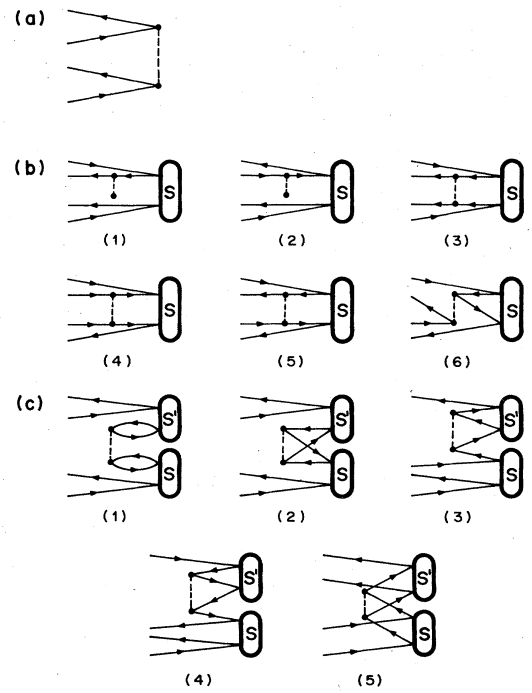

FIG. 10. Schematic representation of mixed Goldstone (interaction vertices) and Hugenholtz (pair-cluster vertices) representation of (a) absolute, (b) linear, and (c) nonlinear CCD diagrams. One Goldstone representative of each such diagram is shown. See. Ref. 50 for details.

where we designated

$$[S]=2S+1\ , \tag{A6}$$

$$\bar{\kappa}=1+\delta_{1,\kappa},\kappa=1,2\ \ (\text{i.e.},\bar{1}=2,\bar{2}=1)\ , \tag{A7}$$

and

$$-F(0)=F(1)=1\ ,\ \ F(2)=\tfrac{1}{3},F(3)=\tfrac{5}{9}\ . \tag{A8}$$

The order of individual terms on the right-hand side of Eqs. (A4) and (A5) corresponds to the order of corresponding diagrams in Figs. 10(b) and 10(c), respectively. The correlation energy is given by the expression

$$\Delta\epsilon=\tfrac{1}{2}\sum_{1',2',1'',2''}\langle 1',2'\,|\,\hat{v}\,|\,1'',2''\rangle \times\sum_{S=0}^{1}(-1)^{1+S}[S]^{1/2}[1,2;1,2]_S\ . \tag{A9}$$

APPENDIX B: SINGULAR BEHAVIOR OF CCD EQUATIONS FOR CYCLIC POLYENES

In this appendix we show that the CCD system, Eq. (29), with the vanishing Jacobian (30) at the critical point $\beta=\beta^0$, Eq. (33), has only complex solutions for $|\beta|<|\beta^0|$, and in the neighborhood of the singularity its Jacobian is proportional to the square root of the resonance-integral difference, Eq. (34).

Designating by x a small change in β about the singular point β^0,

$$x=\beta-\beta^0\ , \tag{B1}$$

we can rewrite the system of CCD equation (29) in the vicinity of β^0 as

$$\tilde{f}_i=f_i+x\tilde{b}_i t_i=0\ ,\ \ i=1,\ldots,m \tag{B2}$$

with f_i given by Eq. (28) and $\tilde{b}_i$ defined by Eq. (27). The singular point $\beta=\beta^0$ is defined by the vanishing of the Jacobian $J(\beta)$, Eq. (30), and we shall assume that the rank of $J(\beta^0)$ is one less than that for $|\beta|>|\beta^0|$, i.e., rank $[J(\beta^0)]=m-1$, while rank $[J(\beta)]=m$ ($|\beta|>|\beta^0|$). This is a plausible assumption since $J(\beta)\neq 0$ for $|\beta|>|\beta^0|$, and the singularity at β^0, where J vanishes, Eq. (33), is its first singularity as the coupling constant is varied from the weakly correlated limit towards the strongly correlated region.

Writing the solution of the system (B2) in the neighborhood of β^0 in the form

$$\underline{t}=\underline{t}^0+\underline{\xi}\ , \tag{B3}$$

and using the fact that $\underline{t}^0$ is a solution at $\beta=\beta^0$, Eq. (32), we can give (B2) the form

$$\Delta\tilde{f}_i(\underline{\xi})=0\ ,\ \ i=1,\ldots,m \tag{B4}$$

with

$$\Delta\tilde{f}_i(\underline{\xi})=x\tilde{b}_i(t_i^0+\xi_i)+(\partial\underline{f}_i,\underline{\xi})+\sum_{j=1}^{m}\sum_{k=1}^{m}c_{ijk}\xi_j\xi_k\ , \tag{B5}$$

where (,) designates an ordinary scalar product,

$$(\partial\underline{f}_i,\underline{\xi})=\sum_{j=1}^{m}b_{ij}\xi_j+2\sum_{j=1}^{m}\sum_{k=1}^{m}c_{ijk}\xi_j t_k^0\ . \tag{B6}$$

It should be noted here that, for the β values away from the singularity, where rank $[J]=m$, we can truncate Eq. (B5) at the first order in x, thus obtaining the solution which is proportional to x and which corresponds to the usual first-order Newton-Raphson procedure. The assumption that rank $[J(\beta^0)]=m-1$ implies the linear dependence of rows $\partial\underline{f}_i\equiv\partial\underline{f}_i(\underline{t}^0)$, so that the constants λ_i exist, not all zero, such that

$$\sum_{i\geq 1}\lambda_i\partial\underline{f}_i=0 \tag{B7}$$

holds. We can assume, without restricting the generality, that $\partial\underline{f}_1\neq 0$ and choose λ_i such that $\lambda_1=1$. We then consider a transformed system

$$\begin{aligned}&\Delta\tilde{f}'_1=\Delta\tilde{f}_1+\sum_{i\geq 2}\lambda_i\Delta\tilde{f}_i=0\ ,\\ &\Delta\tilde{f}'_i=\Delta f_i=0\ ,\ \ i\geq 2\ .\end{aligned} \tag{B8}$$

More explicitly, this new system for the unknown $\underline{\xi}$ can be written as

$$\Delta\tilde{f}'_1=x\tilde{A}_1+x\sum_{j=1}^{m}\tilde{B}_j\xi_j+\sum_{j=1}^{m}\sum_{k=1}^{m}\tilde{C}_{1jk}\xi_j\xi_k=0\ , \tag{B9a}$$

$$\Delta\tilde{f}'_i=x\tilde{b}_i t_i^0+(\partial\underline{f}_i(\underline{t}^0),\underline{\xi})+O(x^2)=0\ ,\ \ i\geq 2 \tag{B9b}$$

where

$$\tilde{A}_1=\tilde{b}_1 t_1^0+\sum_{i\geq 2}\lambda_i\tilde{b}_i t_i^0 ,$$
$$\tilde{B}_1=\tilde{b}_1,\tilde{B}_i=\lambda_i\tilde{b}_i,i\geq 2 , \quad \text{(B10)}$$
$$\tilde{C}_{1jk}=c_{1jk}+\sum_{i\geq 2}\lambda_i c_{ijk} .$$

In Eq. (B9b) we have written out explicitly only the terms which are, at most, linear in x.

Now, considering the linear subsystem for $i\geq 2$, Eq. (B9b), we can write the solution in the form

$$\underline{\xi}=x\underline{\bar{t}}+y\underline{s} , \quad \text{(B11)}$$

where y is an arbitrary parameter, $\underline{\bar{t}}$ is some particular solution of the system

$$\tilde{b}_i t_i^0+(\partial\underline{f}_i(\underline{t}^0),\underline{\bar{t}})=0 , \quad i\geq 2 , \quad \text{(B12)}$$

and $\underline{s}$ satisfies conditions

$$(\partial\underline{f}_i(\underline{t}^0),\underline{s})=0 , \quad i\geq 2 . \quad \text{(B13)}$$

Substituting the solution (B11) into the first equation of our system, Eq. (B9a), and again keeping the terms which are, at most, linear in x, we obtain

$$Ay^2+2Bxy+Cx+O(x^2)=0 , \quad \text{(B14)}$$

where

$$A=\sum_{j=1}^{m}\sum_{k=1}^{m}\tilde{C}_{1jk}s_j s_k ,$$
$$2B=\sum_{j=1}^{m}\tilde{B}_j s_j+2\sum_{j=1}^{m}\sum_{k=1}^{m}\tilde{C}_{1jk}\bar{t}_j s_k , \quad \text{(B15)}$$
$$C=\tilde{A}_1 .$$

Now solving (B14) for y, we obtain

$$y=A^{-1}\{-Bx\pm[(Bx)^2-ACx]^{1/2}\} , \quad \text{(B16)}$$

so that keeping, at most, linear terms in x, we can write

$$y=A^{-1}[-Bx\pm(-ACx)^{1/2}]+O(x^{3/2}) . \quad \text{(B16')}$$

We can now choose x such that

$$-ACx>0 , \quad \text{(B17)}$$

so that y is real, in which case

$$y=A^{-1}(-ACx)^{1/2}+O(x)\approx|x|^{1/2} . \quad \text{(B18)}$$

The Jacobian of the transformed system (B5), which gives the variation δJ of J in the neighborhood of β^0, Eq. (34), is then

$$\tilde{J}=|\partial\tilde{\underline{f}}_i(\underline{t}^0+\underline{\xi})|$$
$$=|\partial\underline{f}_i(\underline{t}^0+\underline{\xi})+x\delta_{ij}\tilde{b}_i|$$
$$=\left|J_{ij}(\underline{t}^0)+2y\sum_{k=1}^{m}c_{ijk}s_k+O(x)\right| , \quad \text{(B19)}$$

and since at least one minor of the order $m-1$ of $J(\beta^0)$ is nonzero, we have that

$$\delta\tilde{J}=\tilde{J}\approx|x|^{1/2}+O(x) , \quad \text{(B20)}$$

thus completing the proof of the assertion (34).

Clearly, when $ACx>0$, which represents β values on the opposite side of β^0 than those given by the condition (B17), only complex solutions will exist.

---

*Also at Department of Chemistry and Guelph-Waterloo Centre for Graduate Work in Chemistry, Waterloo Campus, University of Waterloo, Waterloo, Ontario, Canada N2L 3G1.

†Also at The Laboratory of the National Foundation for Cancer Research, Faculty of Mathematics, University of Waterloo, Waterloo, Ontario, Canada N2L 3G1.

‡Present address: Hi Tech Canada, Ltd., Ottawa, Canada.

[1]E. H. Lieb and D. C. Mattis, *Mathematical Physics in One Dimension* (Academic, New York, 1966).

[2]M. Gaudin, *La Fonction d'Onde de Bethe* (Masson, Paris, 1983).

[3]*One-Dimensional Conductors,* German Physical Society Summer School Proceedings, Vol. 34 of *Lecture Notes in Physics,* edited by H. G. Schuster (Springer, Berlin, 1975); *Quasi-One-Dimensional Conductors I and II,* Proceedings of the International Conference on Quasi-One-Dimensional Conductors, Dubrovnik, Yugoslavia, 1978, Vols. 95 and 96 of *Lecture Notes in Physics,* edited by S. Barišić, A. Bjeliš, J. R. Cooper, and B. Leontić (Springer, Berlin, 1979); *Chemistry and Physics of One-Dimensional Metals,* edited by H. J. Keller (Plenum, New York, 1977); *The Physics and Chemistry of Low Dimensional Solids,* edited by J. Alcacer (Reidel, Dordrecht, The Netherlands, 1980); D. Jerome and H. J. Schultz, Adv. Phys. **31**, 299 (1982).

[4]H. Shirakawa and S. Ikeda, Polym. J. **2**, 231 (1971); H. Shirakawa, T. Ito, and S. Ikeda, *ibid.* **4**, 460 (1973); T. Ito, H. Shirakawa, and S. Ikeda, J. Polym. Sci., Polym. Chem. Ed. **12**, 11 (1974); **13**, 1943 (1975).

[5]H. Shirakawa, E. J. Louis, A. G. MacDiarmid, C. K. Chiang, and A. J. Heeger, J. Chem. Soc., Chem. Commun. **14**, 578 (1977); C. K. Chiang, C. R. Fincher, Jr., Y. W. Park, A. J. Heeger, H. Shirakawa, E. J. Louis, S. C. Gau, and A. G. MacDiarmid, Phys. Rev. Lett. **39**, 1098 (1977); A. J. Heeger and A. G. MacDiarmid, in the *Physics and Chemistry of Low Dimensional Solids,* edited by L. Alcacer (Reidel, Dordrecht, The Netherlands, 1980), p. 353; Y. W. Park, M. A. Druy, C. K. Chiang, A. J. Heeger, A. G. MacDiarmid, H. Shirakawa, and S. Ikeda, J. Polymer Sci., Poly. Lett. **17**, 195 (1979).

[6]C. R. Fincher, Jr., D. L. Peebles, A. J. Heeger, M. A. Druy, Y. Matsumura, A. G. MacDiarmid, H. Shirakawa, and S. Ikeda, Solid State Commun. **27**, 489 (1978); B. R. Weinberger, M. Akhtar, and S. C. Gau, Synth. Met. **4**, 187 (1982); B.R. Weinberger, E. Ehrenfreund, A. Pron, A. J. Heeger, and A. G. MacDiarmid, J. Chem. Phys. **72**, 4749 (1980); S. Ikehata, J. Kaufer, T. Woerner, A. Pron, M. A. Druy, A. Sivak, A. J. Heeger, and A. G. MacDiarmid, Phys. Rev. Lett. **45**, 1123 (1980); M. Nechtshein, F. Devreux, R. L. Greene, T. C. Clarke, and G. B. Street, *ibid.* **44**, 556 (1980), C. B. Duke and H. W. Gibson, in *Kirk-Othmer Encyclopedia of Chemical Technology,* 3rd ed. (Wiley, New York, 1982), Vol. 18, p. 755

and references therein.
[7]W. P. Su, J. R. Schrieffer, and A. J. Heeger, Phys. Rev. Lett. **42**, 1698 (1979), M. J. Rice, Phys. Lett. **71A**, 152 (1979); S. Brazovskii, Zh. Eksp. Teor. Fiz. Pis'ma Red. **28**, 606 (1978) [JETP Lett. **28**, 656 (1978)]; Zh. Eksp. Teor. Fiz.**78**, 677 (1980) [Sov. Phys.—JETP **51**, 342 (1980)].
[8]B. Hudson and B. Kohler, Ann. Rev. Phys. Chem. **25**, 437 (1974); B. S. Hudson, B. E. Kohler, and K. Schulten, in *Excited States,* edited by E. C. Lim (Academic, New York, 1982), Vol. 6.
[9]A. A. Ovchinikov, I. I. Ukrainskii, and G. V. Kventzel, Usp. Fiz. Nauk **108**, 81 (1972) [Sov. Phys.—Usp. **15**, 575 (1973)].
[10]K. Schulten, I. Ohmine, and M. Karplus, J. Chem. Phys. **64**, 4422 (1976); I. Ohmine, M. Karplus, and K. Schulten, *ibid.* **68**, 2298 (1978); P. Tavern and K. Schulten, *ibid.* **70**, 5407 (1979).
[11]F. A. Matsen, Acc. Chem. Res. **11**, 387 (1978).
[12]I. I. Ukrainskii, Zh. Eksp. Teor. Fiz. **76**, 760 (1979) [Sov. Phys.—JETP **49**, 381 (1979)].
[13]P. Horsch, Phys. Rev. B **24**, 7351 (1981).
[14]S. Kivelson and D. Heim, Phys. Rev. B **26**, 4278 (1982).
[15]H. Fukutome and M. Sasai, Prog. Theor. Phys. **67**, 41 (1982).
[16]L. R. Ducasse, T. E. Miller, and Z. G. Soos, J. Chem. Phys. **76**, 4094 (1982); Z. G. Soos and S. Ramasesha, Chem. Phys. Lett. **101**, 34 (1983); Phys. Rev. Lett. **51**, 2374 (1983); Phys. Rev. B **29**, 5410 (1984).
[17]J. Paldus and M. J. Boyle, Int. J. Quantum Chem. **22**, 1281 (1982); for $N=6$ case, also see J. Paldus, J. Čížek, and L. Šroubková, Coll. Czech. Chem. Commun. **36**, 618 (1971), J. Čížek, J. Paldus, L. Šroubková, and J. Vojtík, *ibid.* **36**, 599 (1971); J. Čížek, J. Paldus, and L. Šroubková, Int. J. Quantum Chem. **3** 149 (1969).
[18](a) J. Paldus and E. Chin, Int. J. Quantum Chem. **24**, 373 (1983); (b) J. Paldus, E. Chin, and M. G. Grey, *ibid.* **24**, 395 (1983); (c) R. Pauncz and J. Paldus, *ibid.* **24**, 411 (1983); (d) J. Paldus and M. Takahashi, *ibid.* **25**, 423 (1983); (e) M. Takahashi and J. Paldus, *ibid.* **26**, 349 (1984).
[19]M. Takahashi, J. Paldus, and J. Čížek, Int. J. Quantum Chem. **24**, 707 (1983).
[20]S. N. Dixit and S. Mazumdar, Phys. Rev. B **29**, 1824 (1984); S. Mazumdar and S. N. Dixit, Phys. Rev. Lett. **51**, 292 (1983); Phys. Rev. B **29**, 2317 (1984).
[21]J. Paldus and J. Čížek, Phys. Rev. A **2**, 2268 (1970).
[22]M. Bénard and J. Paldus, J. Chem. Phys. **72**, 6546 (1980).
[23]F. E. Harris and J. Delhalle, Phys. Rev. Lett. **39**, 1340 (1977); J. Delhalle and F. E. Harris, Theor. Chim. Acta **48**, 127 (1978).
[24]J.-L. Calais, Ark. Fys. **28**, 11 (1965); K. F. Berggren and F. Martino, Phys. Rev. **184**, 484 (1969); M. Kertész, J. Koller, and A. Ažman, Phys. Rev. B **19**, 2034 (1979); A. Karpfen, Chem. Phys. Lett. **61**, 363 (1979); J.-M. André, J.-L. Brédas, J. Delhalle, Y. Kalenov, L. Piela, and J.-L. Calais, Int. J. Quantum Chem. Symp. **14**, 419 (1980).
[25]L. Piela, J.-M. André, J.-L. Brédas, and J. Delhalle, Int. J. Quantum Chem. Symp. **14**, 405 (1980).
[26]S. Suhai, J. Chem. Phys. **73**, 3843 (1980); Chem. Phys. Lett. **96**, 619 (1983); Phys. Rev. B **27**, 3506 (1983); Int. J. Quantum. Chem. **23**, 1239 (1983).
[27]R. S. Jones and S. B. Trickey, J. Phys. C (to be published).
[28]D. L. Freeman, Phys. Rev. B **15**, 5512 (1977).
[29]R. F. Bishop and K. H. Lührmann, Phys. Rev. B **17**, 3757 (1978); **26**, 5523 (1982), and references therein.
[30]J. Paldus, J. Čížek, and M. Takahashi, Phys. Rev. A (to be published).
[31]J. Čížek, J. Chem. Phys. **45**, 4256 (1966).
[32]K. Jankowski and J. Paldus, Int. J. Quantum Chem. **18**, 1243 (1980).
[33](a) B. G. Adams, K. Jankowski, and J. Paldus, Phys. Rev. A **24**, 2316 (1981); (b) *ibid.* **24**, 2330 (1981).
[34]R. A. Chiles and C. E. Dykstra, Chem. Phys. Lett. **80**, 69 (1981).
[35]J. Hubbard, Proc. R. Soc. London, Ser. A **240**, 539 (1957); **243**, 336 (1958); **244**, 199 (1958).
[36]N. M. Hugenholtz, Physica (Utrecht) **23**, 481 (1957).
[37]F. Coester, Nucl. Phys. **7**, 421 (1958); F. Coester and H. Kümmel, *ibid.* **17**, 477 (1960).
[38]J. Čížek, Adv. Chem. Phys. **14**, 35 (1969).
[39]R. J. Bartlett, C. E. Dykstra, and J. Paldus, in *Vectorization of Advanced Methods for Molecular Electronic Structure,* proceedings of the NATO Advanced Research Workshop, edited by C. E. Dykstra, R. Ahlrichs, and W. Meyer (Reidel, Dordrecht, The Netherlands, in press).
[40]J. Paldus, in *New Horizons of Quantum Chemistry,* edited by P.-O. Löwdin and B. Pullman (Reidel, Dordrecht, The Netherlands, 1983), p. 31.
[41]V. Kvasnička, V. Laurinc, S. Biscupič, and M. Haring, Adv. Chem. Phys. **52**, 181 (1983); V. Kvasnička, V. Laurinc, and S. Biskupič, Phys. Rep. **90**, 159 (1982).
[42]R. J. Bartlett, Ann. Rev. Phys. Chem. **32**, 359 (1981).
[43]J. Čížek and J. Paldus, Phys. Scr. **21**, 251 (1980); J. Čížek, in *Quantum Theory of Polymers,* edited by J.-M. André, J. Delhalle, and J. Ládik (Reidel, Dordrecht, The Netherlands, 1978), p. 103.
[44]H. Kümmel, K. H. Lührmann, and J. G. Zabolitzky, Phys. Rep. **36**, 1 (1978).
[45]I. Lindgren and J. Morrison, *Atomic Many-Body Theory* (Springer, New York, 1982).
[46]J. Paldus, and J. Čížek, Adv. Quantum Chem. **9**, 105 (1975); J. Paldus, *Diagrammatical Methods for Many-Fermion Systems* (Lecture Notes, University of Nijmegen, Holland, 1981).
[47]Compare, e.g., J. Paldus, in *Theoretical Chemistry: Advances and Perspectives,* edited by H. Eyring and D. J. Henderson, (Academic, New York, 1976), Vol. 2, p. 131.
[48]J. Čížek and J. Paldus, Int. J. Quantum Chem. **5**, 359 (1971).
[49]J. Paldus, B. G. Adams, and J. Čížek, Intern. J. Quantum Chem. **11**, 813 (1977); J. Čížek, Theor. Chim. Acta **6**, 292 (1966).
[50]J. Paldus, J. Chem. Phys. **67**, 303 (1977).
[51]E. El Baz and B. Castel, *Graphical Methods of Spin Algebras in Atomic, Nuclear and Particle Physics* (Dekker, New York, 1972).
[52]J. Paldus, P. E. S. Wormer, F. Visser, and A. van der Avoird, J. Chem. Phys. **76**, 2458 (1982).
[53]S. M. Backrach, R. A. Chiles, and C. E. Dykstra, J. Chem. Phys. **75**, 2270 (1981).
[54]J. Paldus, P. E. S. Wormer, and M. Bénard, unpublished results.
[55]P.-O. Löwdin, Phys. Rev. **97**, 1509 (1955); J. Appl. Phys. Suppl. **33**, 251 (1962); Rev. Mod. Phys. **34**, 520 (1962); Adv. Chem. Phys. **14**, 283 (1969).
[56]P.-O. Löwdin, *Symposium on Molecular Physics* (Maruzen, Tokyo, 1953), p. 13.
[57]R. Pauncz, *Alternant Molecular Orbital Method* (Saunders, Philadelphia, 1967).
[58]R. Pauncz, J. de Heer, and P.-O. Löwdin, J. Chem. Phys. **36**, 2247 (1962); J. de Heer and R. Pauncz, J. Mol. Spectrosc. **5**, 326 (1960).
[59]R. G. Parr, *The Quantum Theory of Molecular Electronic*

Structure (Benjamin, New York, 1963).
[60]N. Mataga and K. Nishimoto, Z. Phys. Chem. **13**, 140 (1957).
[61]J. Paldus, J. Čížek, and I. Hubač, Int. J. Quantum Chem. Symp. **8**, 293 (1974).
[62]J. Čížek, F. Hashimoto, M. Takahashi, and J. Paldus, unpublished results.
[63]E. H. Lieb and E. Y. Wu, Phys. Rev. Lett. **20**, 1445 (1968).
[64]R. W. H. Cho, M. Math. thesis, University of Waterloo, 1981.
[65]T. P. Zivković and H. J. Monkhorst, J. Math. Phys. **19**, 1007 (1978).
[66]J. Paldus, M. Takahashi, and R. W. H. Cho, Int. J. Quantum Chem. Symp. (to be published).
[67]J. Paldus, J. Čížek, and J. Shavitt, Phys. Rev. A **5**, 50 (1972).
[68]J. Paldus, J. Čížek, and A. Laforgue, Int. J. Quantum Chem. **13**, 41 (1978).
[69]J. Čížek and J. Paldus, J. Chem. Phys. **47**, 3976 (1967).
[70]J. Paldus and M. G. Grey, unpublished results; M. G. Grey, M.Sc thesis, University of Waterloo, 1982.
[71]P. E. S. Wormer, *Different Orbitals for Different Spins* (Afstudeerverslag, Technological University Delft, Delft, The Netherlands, 1969); P. E. S. Wormer and A. van der Avoird, Int. J. Quantum Chem. **8**, 715 (1974).
[72]A. Pellégatti, J. Čížek, and J. Paldus, J. Chem. Phys. **60**, 4825 (1974); Int. J. Quantum Chem. **21**, 147 (1982); K. Hashimoto, J. Čížek, M. Takahashi, and J. Paldus, unpublished results.
[73]M. Takahashi, Prog. Theor. Phys. **45**, 756 (1971); I. A. Misurkin and A. A. Ovchinnikov, Teoret. i Mat. Fiz. **11**, 127 (1972).